Applied Thermal Engineering 209 (2022) 118235

Contents lists available at ScienceDirect

Applied Thermal Engineering

journal homepage: www.elsevier.com/locate/apthermeng

Objective oriented phase change material composite heat sink design

Alison Hoe [a], Michael T. Barako [b], Achutha Tamraparni [c], Chen Zhang [d], Alaa Elwany [d], Jonathan R. Felts [c], Patrick J. Shamberger [a,*,1]

[a] Department of Materials Science and Engineering, Texas A&M University, College Station, TX, United States
[b] NG Next Basic Research Laboratory, Northrop Grumman Corporation, Redondo Beach, CA, United States
[c] Department of Mechanical Engineering, Texas A&M University, College Station, TX, United States
[d] Department of Industrial and Systems Engineering, Texas A&M University, College Station, TX, United States

ARTICLE INFO

Keywords:
Composite Design
Electronics Cooling
Thermal Management
Thermal Energy Storage
Applied Phase Change Materials

ABSTRACT

While phase change material based heat sinks have been shown to act as highly efficient transient cooling devices, the effective implementation of these components is prevented by a lack of design guidelines. Here, we develop an analytical framework for optimizing the design of rectangular and cylindrical phase change material composite heat sinks. This is accomplished through the definition of two design objectives: (1) maximize thermal buffering capacity at a given time, and (2) maximize the time the system can achieve a minimum thermal buffering capacity threshold. In this context, thermal buffering capacity can be quantified in terms of heat absorption rate or temperature, depending on the boundary condition applied. We demonstrate that, in finite volumes, there exist two design regimes where the thermal buffering capacity is either limited by the rate at which the system can absorb thermal energy or by the total thermal capacitance of the system. We present analytical expressions describing the optimal volume fraction for each combination of design objectives, form factors, and boundary conditions derived from appropriate analytical solutions for the melting problem. Analytically predicted optimal volume fractions are validated with numerical and experimental results from existing literature and original work. This collective toolbox enables thermal engineers to make rational decisions on architecture to optimize components under specific thermal loads and specific system constraints.

1. Introduction

Thermal energy storage (TES) systems containing phase change materials (PCMs) have been established as highly efficient components for transient cooling [1,2] but are hindered by a lack of cohesive geometry and composition design guidelines, resulting in underperforming PCM structures developed through arbitrary or empirical methods. While the basic principles of heat transfer during melting and solidification processes are well-understood [3-5], the translation of the fundamental physics into rational module design principles for this type of nonlinear thermal device are not well-defined. This is contrasted with other common thermal management components such as heat sinks [6,7], heat pipes [8-10], heat exchangers [6,11] which have had extensive development of definite design principles. TES systems can be primarily defined by their (1) power density, which describes the rate of heat transfer through the material, and their (2) energy density, which quantifies the amount of the thermal energy that can be absorbed [12-15]. Phase change materials (PCMs) are notable for their high energy density, which can be utilized through the phase transition, but are often lacking in power density [12,16]. As a result, it is often desirable to combine high thermal conductivity materials with PCMs to form high performance composites, within which the composition or structure may be tuned to modify resultant system properties [13,15]. Currently, it is not understood how composition and architecture can be used to select for a chosen response profile or thermal buffering capacity under realistic application constraints.

Thermal buffering capacity is a term which can be used as a description of the performance of a TES cooling device, which describes a TES system's ability to dampen transient thermal loads and can be considered in terms of heat absorption rate or temperature, depending on the boundary condition applied. The characteristic response of a standard PCM system is demonstrated schematically in Fig. 1a under an applied heat flux thermal load, and in Fig. 1b for an applied constant temperature thermal load. For constant boundary conditions with an applied constant temperature thermal load, the heat flux into the

* Corresponding author.
E-mail address: patrick.shamberger@tamu.edu (P.J. Shamberger).
[1] Reed-McDonald Bldg, 575 Ross St, College Station, TX 77840, United States.

https://doi.org/10.1016/j.applthermaleng.2022.118235
Received 11 August 2021; Received in revised form 24 December 2021; Accepted 16 February 2022
Available online 19 February 2022

Nomenclature

Variables

C_p	Specific heat at constant pressure, $(Jkg^{-1}K^{-1})$
f	Melt fraction
k	Thermal conductivity, $(Wm^{-1}K^{-1})$
L_v	Volumetric latent heat of fusion, (Jkg^{-1})
q''	Heat flux,(Wm^{-2})
r	Radius,(m)
Ra	Rayleigh number, (unitless)
St	Stefan number, (unitless)
t	Time,(s)
T	Temperature,(C)
y	Vertical location,(m)
δ	melt front location,(m)
ρ	Density,(kgm^{-3})
ϕ	Volume fraction, (unitless) Intrinsic material property

Subscripts

0	At heated boundary, y = 0 or r = r_0
cart	Based in Cartesian coordinates
cyl	Based in Cylindrical coordinates
eff	Effective
f	Farthest edge of system
i	Constituent index
l	Of the liquid
m	Melting
metal	Metal
OPT	Optimal
PCM	Phase change material
thresh	Threshold

material system is an appropriate performance metric for thermal buffering capacity, whereas for an applied heat flux thermal load the temperature of the heated boundary is the appropriate choice.

Composite materials can be defined as systems containing two or more components, where the properties of those materials can be combined to calculate a set of effective properties which accurately model the composite's macroscopic behavior. PCM composite systems take many geometries which most often fall into the categories of: composite dispersions [17-20], macro-/micro- porous media (eg. lattices or foams) [13,21-25] , and finned heat sinks [26-28]. Additionally, composites systems can also be formed using combinations of characteristic elements from these categories such as the fins and foams [29-

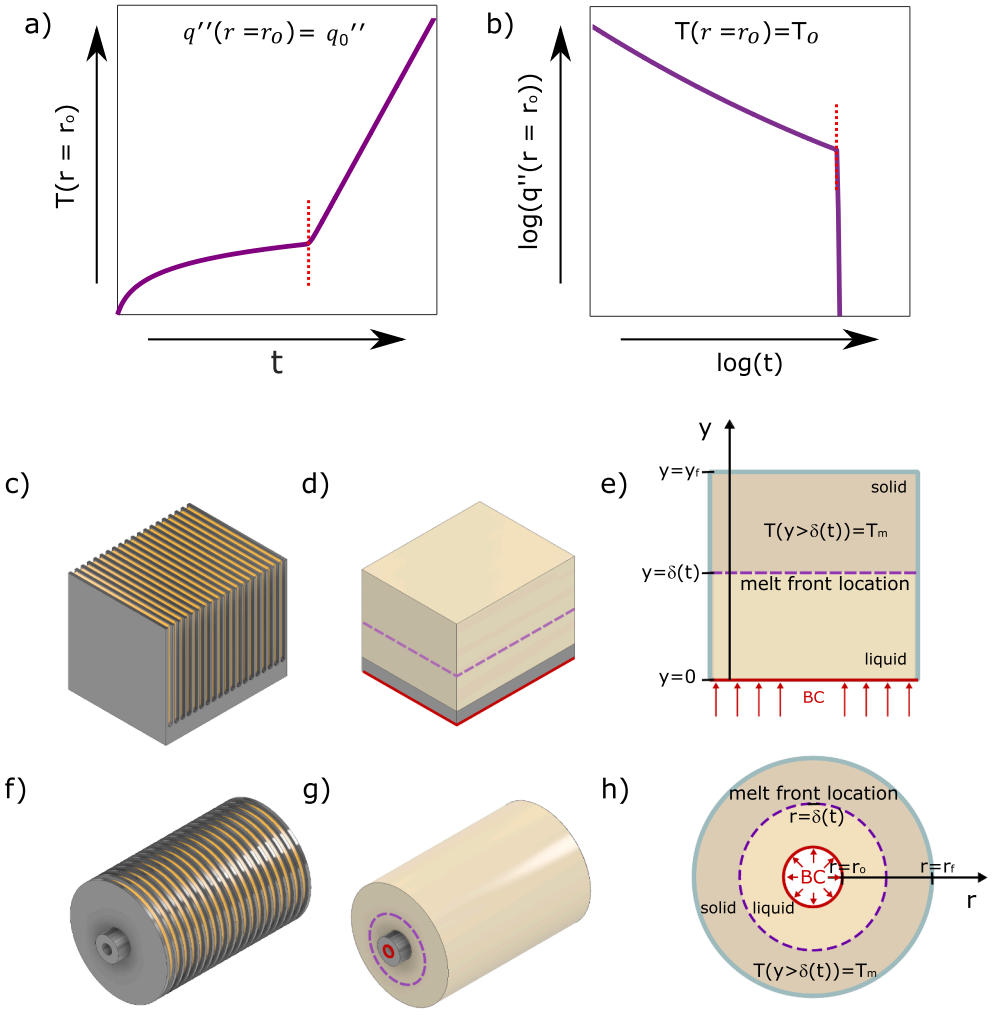

Fig. 1. Characteristic responses of PCM volumes to an applied a) heat flux (q″) or b) temperature (T) boundary condition with the melting completion time indicated with a red dashed line. Schematic of c,f) finned composite system, approximated as a d,g)homogeneous composite and, e,h) fundamental configuration of the thermal problem with a c,d,e) Cartesian and f,g,h) cylindrical coordinate basis. Solid red lines indicate the boundary where the thermal load is applied, and the dashed purple lines indicate the uniformly distributed melt front location. (For interpretation of the references to colour in this figure legend, the reader is referred to the web version of this article.)

31] or fins and dispersions [32-34]. Each category metal/PCM assemblies can be described as an ideal composite in the limit of small constituent spacing, where the length scales of heat transfer between the conductive material and the PCM become sufficiently small such that the temperature profile is effectively even and moves as a uniform front [35-38]. One advantage of treating the system as a homogeneous material is the resulting simplification of the melting problem from a 3D, or 2D, configuration (Fig. 1c,f) to a 1D configuration (Fig. 1d,g). This saves significant computational expense in numerical simulations, allowing for rapid testing of varying configurations and presents the opportunity for simplified analytical solutions to non-trivial configurations and scenarios, as detailed in the following sections. This approximation will break down in the presence of high convective driving forces, associated with large Rayleigh ($Ra > 10^6$, for systems with high effective thermal conductivity) [39,40], and in cases of wide constituent spacing [35,37]. However, with this limitation being known, constituent spacing can be selected such that the requirement of small spacing is met and when this is true, even with relatively high driving forces, the role of convection has been shown to play a very small role in comparison to conductive forces [27,41].

When designing PCM composite systems, the proportion and configuration of components within these structures directly dictates the direction and magnitude of heat transfer within the system [13,14]. The most common thermal management components are rectangular slabs, corresponding to planar heat sources, or cylindrical annuluses, corresponding to line or circular pipe heat sources, both of which are investigated in this work. These systems are commonly filled with rectangular or radial fins (Fig. 1c,f), respectively, because they are easily manufactured and can access a large range of volume fractions, which are inaccessible by nanocomposites [20] or more complex structures [13,42]. These structures also represent the upper limit of anisotropic heat transfer parallel to the direction of heat flow [43].

The bulk of previous work on PCM composite design has focused on experimental or numerical empirical testing of similar geometries and selecting the highest performing system within a sample set of thermal configurations [28,41,44-46]. Differing thermal configurations can be defined as permutations of materials, boundary conditions, time scales, coordinate bases, critical performances metrics, thermal loading, and length scales, where each configuration will correspond to a specific optimal design. These empirical studies only provide limited insight into the characteristics of specific high-performance systems by optimizing a particular subset of thermal configurations, but their results do not provide widely applicable design guidelines for the broader design space. Moreover, the data provided in these studies is sparse in comparison to the overall degrees of freedom in the design space. Therefore, these studies are unlikely to identify underlying correlations and design rules.

Analytical optimization efforts often focus on identifying useful figures of merit which identify the point of component mixing where the thermally capacitive and conductive elements best balance each other to maximize the rate of heat absorption from the heated boundary under simple thermal loads [13,47,48]. These approaches are useful as a starting place for PCM based designs, but these solutions assume a quasi-infinite volume, therefore not accounting for geometric constraints or efficient utilization of allotted space. This assumption is sufficient for lower power applications, and very large available volumes, but for most real-world design applications, it becomes necessary to account for finite available volumes. The otherwise lack of sensitivity toward finite volumes in the literature is partially addressed in work by Lu through the development of a methodology to select for allowable heat pulses for a given PCM body with specified geometry and an upper threshold temperature limit [49]. While this methodology is useful for determining operating parameters, it is not trivial to translate to system design and is limited to the selection of constant heat flux pulses in Cartesian coordinates and only explores one optimization goal.

For finite volumes, the time corresponding to the completion of melting marks the point where subsequent times experience a rapid decrease in performance for both thermal load types and corresponds to the limit of the PCM's thermal buffering capacity (Fig. 1a,b) [35]. Previous work by Bransier found that this point of melting completion could be used as a design tool for dimension selection [50]. The author showed that the width of a PCM slab, perpendicular to a planar thermal load, should be chosen such that the time at which optimization is occurring should correspond to the complete melting of the system. This emphasizes the impact the constraint of a finite volume places on the design problem, which is very common in application.

In this work we seek to develop a methodology that will allow the tailoring of a specific thermal response through composition selection of the thermally conductive and capacitive elements in a dynamic PCM thermal system. Furthermore, we seek to address the role of a volume constraint on the resulting optimization, as this is a facet of the design problem that is not often addressed by current literature, but is critical for most applications. To this end, we establish a comprehensive analytical framework describing this optimal composition for highest thermal buffering capacity with the objective to either 1) maximize the thermal buffering of the heated boundary at a given time, or 2) maximize the time the desired buffering effect occurs. To ensure the widespread applicability of this work, the breadth of our frameworks includes constant temperature and constant heat flux boundary conditions, where we consequently analyze thermal buffering in terms of the complementary boundary variable not being fixed. We also complete our analysis for both Cartesian and cylindrical based systems, allowing this work may be applied to a large variety of applications. For each combination of coordinate systems, performance metrics, and boundary conditions, an optimal volume fraction is analytically identified and compared against analogous numerical and experimental results, both from the existing body of literature and original results. The analytical solutions contained herein are meant to provide a practical guideline for the design of PCM composite systems for thermal management when the application is known. This provides an unprecedented degree of design insight currently lacking in the current literature, especially considering the breadth of thermal configurations and design objectives contained in this work.

2. Methods

2.1. Problem statement

In the pursuit of optimal composite design, we consider the composite to act as a singular effective medium through the homogeneous composite approximation ($\oint$ **3.1.2**) and utilize the quasi-steady state (QSS) approximation ($\oint$ **3.1.3**) to describe internal heat transfer and melt dynamics.

The system of study is initially defined at the melting point, entirely in the solid state. The appropriate heating boundary condition of either a constant temperature or heat flux is applied to a single boundary and all other boundaries are adiabatic (Fig. 1e,h). It is assumed in our analytical and numerical approaches that the solid and liquid phases are distinct and their respective material properties are not dependent on temperature. Furthermore, convective heat and mass transfer are considered negligible in our model, confining heat transfer to conductive pathways, which is practical for the small length scales we are considering. At such length scales, where the composite approximation is most valid, the associated Rayleigh numbers become relatively small, indicating negligible levels of convective heat transfer, as previously discussed [39]. In this limit, the interaction between fluid viscosity and geometric confinement balances the buoyant forces and convective heat transfer is dwarfed by conductive heat transfer [27,40,41]. Furthermore, this is also the limit in which the time for heat penetration from the conductive fin into the PCM becomes increasingly small and the thermal front converges to a uniform distribution, consistent with a singular effective medium [35,36]. As volume fraction limits to 0, where there is no metal

in the system, a manufacturability limit will be reached, and our assumptions will break down. However, if a design problem yields a solution with the sole goal of increasing thermal capacitance, the singularly PCM system is expected to still be the highest performing solution.

The material composites developed and analyzed herein are composed of octadecane and aluminum alloy, AlSi12 (Table 1). Octadecane was chosen for its near room temperature melting point, high latent heat, and ease of incorporation. In our analytical and numerical models, the melting temperature is approximated as a single well-defined temperature which is an assumption that varies in accuracy depending on the PCM in question. Octadecane is known to melt over a range of temperatures which can vary depending on the sample purity. For the material used in this study, the full width at half maximum range of the melting peak was measured with DSC to be 3.3 ℃ for a moderate heating rate of 10 ℃/min, which is relatively small when compared to the total heating range under investigation here. This demonstrates that while approximating the melting temperature as discrete adds a level of approximation to our experimental comparisons, it is still a reasonable approximation to make and we have observed that using a low value within the melting range has shown strong comparisons to experimental results. AlSi12 was chosen for our related additive manufacturing capabilities and for its high thermal conductivity. To manufacture optimally performing systems, the aluminum alloy structures are designed through the analytical optimization system described herein, these structures are then manufactured by powder bed laser fusion and infiltrated with octadecane, as further discussed in section § **2.3**.

2.2. Finite difference analysis

In this work, numerical investigations are utilized to characterize heat transfer and, specifically, the time-dependent temperature rise, and quantity of heat absorbed by a composite PCM volume under externally applied boundary conditions. We use 1D finite difference analysis (FDA) models simulating conductive heat transfer through Cartesian and cylindrical PCM composite geometries, which have been established and tested in previous work (Fig. 2) [35,36,51]. The fundamental assumptions of the FDA models include 1) the material properties of the solid and liquid phases are not dependent on temperature, 2) melting occurs at a singular temperature, 3) the interface between phases is well-defined, 3) the densities of the solid and liquid phases are equal leading to no mass transfer upon phase change and 4) no convection occurs in the liquid phase. These assumptions also carry through to the analytical models contained in this work.

Within the FDA, nodes are linearly spaced between boundaries and node characteristics are given by the system geometry and effective properties (Eqs. (3), (4), Fig. 2). For all simulations executed in this work, the initial state of the bulk is completely in the solid state and held at the melting temperature. A singular boundary node is set to apply a thermal load of either an applied constant heat flux or temperature and the opposing boundary node is adiabatic. For every timestep, the heat transfer between nodes is calculated using an implicit backward Euler method, from which the temperature and melt fraction of each node is determined. To this end, for a Cartesian coordinate basis the heat

Table 1
Material properties used in original numerical simulations and analytical modelling.

	Units	AlSi12 alloy	Octadecane
k_l	$Wm^{-1}K^{-1}$	–	0.15
k_s	$Wm^{-1}K^{-1}$	80	0.36
L_v	$J\ m^{-3}$	–	1.74 x10^8
ρ	kgm^{-3}	2700	712
C_p	$Jkg^{-1}K^{-1}$	900	2200
T_m	C	–	28

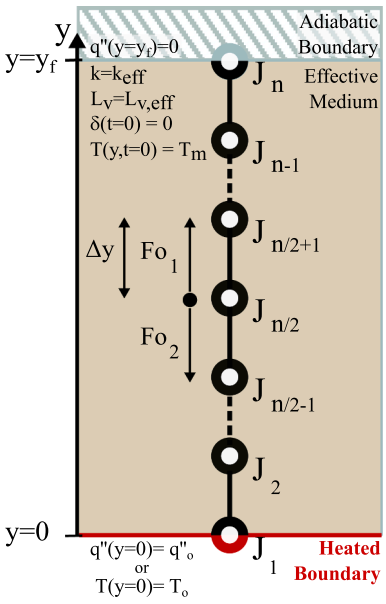

Fig. 2. Schematic visualization of the computational space under consideration demonstrating the setup of the system and the means for using Fourier numbers (Fo) to simulate heat transfer between evenly spaced (Δy) nodes (J_1 – J_n) from the heated boundary (J_1) to the adiabatic boundary (J_n).

equation is given by:

$$\frac{1}{\partial y}\left(k\frac{\partial T}{\partial y}\right)=\rho C_p\frac{\partial T}{\partial t}+L_v\frac{\partial f}{\partial t} \tag{1}$$

where y, ρ, C_p, T, t, k and L_v represent distance, density, specific heat capacity, temperature, time, thermal conductivity, and volumetric latent heat, respectively [6]. The melt fraction of a given node volume is represented by f, where the possible values are; 0 which represents not at all melted, 1 which represents completely melted and intermediate values represent partial melting. Within Eq. (1) the left-hand side of the equation represents the rate of heat transfer through the given volume and the right-hand side of the equation represents the heat absorbed by the volume through sensible (term 1) and latent (term 2) heating. The same concepts of energy conservation can also be applied to a cylindrical coordinate basis, yielding the heat equation:

$$\frac{1}{r}\frac{1}{\partial r}\left(kr\frac{\partial T}{\partial r}\right)=\rho C_p\frac{\partial T}{\partial t}+L_v\frac{\partial f}{\partial t} \tag{2}$$

where the r is radial distance [6]. Within the FDA, once the melting temperature of a given node is reached, the node will absorb thermal energy into the latent heat until the volume is completely melted before beginning to sensibly heat leading to a singular well-defined front.

Fidelity of FDA model is directly dependent on timestep length and node spacing. Timesteps are chosen to be most fine at earliest times (10^{-7} s) increasing by 10^{-7} s each step. A total of 2000 nodes are distributed between the two boundaries of the simulated volume. This combination of values yields the highest relationship between fidelity and computational expense. Timesteps and number of nodes were chosen such that full convergence was observed between tests of increasingly smaller timesteps and larger number of nodes. Accuracy of the resulting finite difference model was tested against ANSYS simulations, analytical models, and experimental data [35,51]. Simulated heat transfer continues until an end condition is met, determined by the thermal conditions and objective function being designed for, as a given time or performance threshold.

2.3. Experimental verification

To supplement thorough numerical testing, a set of experimental

tests are done to further validate the proposed analytical framework. Cylindrical metal finned structures are fabricated from Aluminum alloy, AlSi12 (3D Systems, PS2585-18), using laser powder bed fusion (ProX 200), which is selected for its ability to generate high resolution features (beam spot diameter: 80 μm) with low porosity (<1 vol%). The metal structures are longitudinally uniform with radially branching fins designed to maintain a target uniform volume fraction throughout the cylindrical volume, while maintaining a maximum spacing of 1 mm in order to satisfy the composite effective properties assumption [35,52]. These cylindrical structures are designed with consistent parameters: 38.1 mm axial length, 3.6 mm inner radius, 1.5 mm metal base width and outer radius of 19.1 mm, with a maximum uncertainty of ± 0.2% on all fabrication dimensions. Metal structures are filled with molten PCM and refrigerated to solidify.

Insulating layers of silicone foam are used to enclose the experimental test rig and prevent environmental heat transfer. Cylindrical composites are initial initially held isothermally at 22 °C where all the PCM is in the solid state. A cartridge heater is used to apply a constant heat flux thermal load of 7.3 ± 0.3 W·cm^{-2} to the inner radius of the cylindrical composite (CIR-10151/120 V, Omega), where the uncertainty represents the combined uncertainty of the cartridge heater surface area and the measured heater power. Thermistors, with a variability of ± 1 ℃, are attached to inner wall of the composite and are used to record temperature while the system undergoes heating (MP3022, TE Tech) [52].

3. Theoretical development

3.1. Analytical foundation

3.1.1. Limiting regimes

Within this work, for every configuration of interest we define an individual solution for the *rate limited* and *volume limited* regimes. These solutions are presented as optimal volume fractions, ϕ, which refer specifically to the volume fraction of metal within the system. In the *rate limited* regime, the performance of the system is limited by the rate at which heat can be absorbed into the system. The *rate limited* regime case is effectively equivalent to an infinite medium because the melt front has no interaction with the edges of the system. Consequently, in this case it may be recommended that the system size be decreased to cut down on the total mass and volume of the thermal management system and cut down on unused volumes. Fig. 3 (c,d) demonstrates that the *rate limited* optimum is the absolute optimal performance the system may have to a thermal load.

When a volume constraint is taken into account, the composition predicted by using a *rate limited* calculation may no longer be optimal (Fig. 3c,d), leading to the definition of a second regime designated as the *volume limited* regime. Since the *rate limited* optimum does correspond to the highest possible performance given no volume constraints, it follows that a system designer may wish to relax volume constraints to achieve the highest performance optimum if possible. However, in many cases volume constraints may be inflexible and using the *rate limited* optimum would lead to extremely poor performance, which emphasizes the importance of utilizing the *volume limited* regime when necessary. In this case the performance is now limited by the total thermal capacity of the system and the optimum is determined by the composition leading to full utilization of the volume (Fig. 3a-b). The primary objective of the

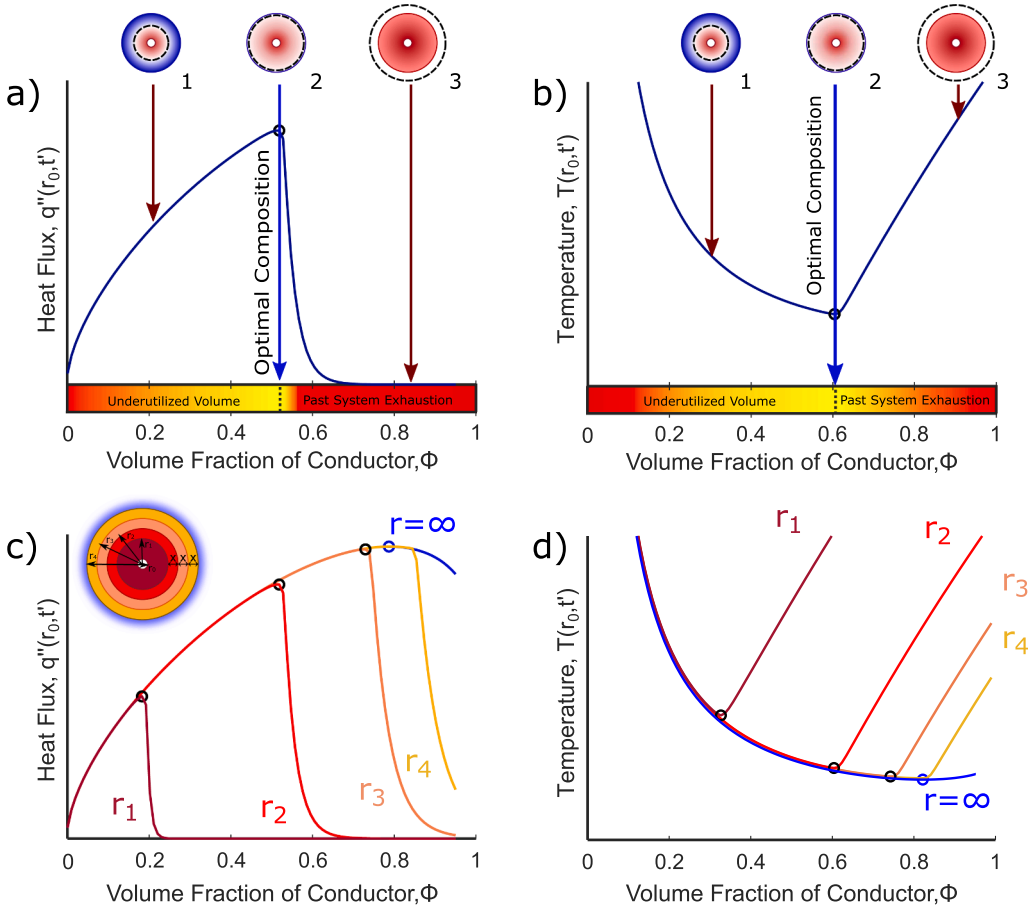

Fig. 3. Compositional dependence of a) final heat flux, when a constant temperature boundary condition is applied ($T(r = r_0) = T_0$), and b)final temperature, when a constant heat flux boundary condition is applied ($q''(r = r_0) = q_0''$), at time, t′, with respect to the volume fraction of metal ϕ. d) For a series of varying radii, the compositional dependence of performance at a given time is explored for e) constant temperature and f) constant heat flux boundary conditions. In the volume limited regime (r_1, r_2, r_3), the optimal composition is affected by the finite boundary and in the rate limited regime (r_4), the optimal composition coincides with an infinite system.

volume limited regime is to add additional capacitance preventing the onset of detrimental effects of melting completion. This leads to a decrease in volume fraction with increasing times of interest or thermal loading magnitude.

The optimal composition is dependent on problem specific factors such as, material properties, geometric constraints, performance metric and thermal loading. Once the thermal and geometric parameters of the optimization problem are defined, the *rate limited* optimum, and the *volume limited* optimum should both be calculated and the lesser of the two values should be selected as the true optimum (Fig. 3c-d).

3.1.2. Homogeneous composite approximation

The homogenous composite approximation treats a multicomponent material system as a single medium, where the effective properties are calculated from: the constituent material properties, the relative volume fraction of constituent components, and their distributions. Previous literature has shown that in the effective medium limit, where decreased the constituent components are well-mixed and separated by small length scales, thermal transport in PCM systems can be calculated using the homogeneous composite approximation [35-37,53]. As previously discussed, for such composites, this limit corresponds to behavior where the time for heat penetration from the conductive fin into the PCM becomes increasingly small and convective heat transfer is dwarfed by conductive heat transfer [35,40]. The homogeneous composite approximation represents the upper limit of heat transfer for these systems and defines the objective of optimizing composnent spacing within a composite, i.e. optimal component spacing corresponds to the limit where performance converges with the homogeneous composite model [13,35,36]. The validity of this approximation has been demonstrated in both Cartesian and cylindrical coordinate systems [35,37], and the critical point of spacing for use of this approximation is analytically described for Cartesian systems [35].

For intrinsic properties, the resulting effective properties are determined solely through constituent volume/proportions, whereas extrinsic transport properties, such as thermal conductivity, also consider the specific internal geometries. For intrinsic properties, the effective property, X_{eff}, can be calculated as:

$$X_{eff} = \sum_i \phi_i X_i \tag{3}$$

where each constituent volumetric material property, X_i, is scaled by the constituent volume fraction, ϕ_i [54]. For the case of heat transport parallel to the heat source the effective thermal conductivity, k_{eff}, follows the upper bound associated with conductive elements arranged in parallel along the direction of heat transfer and can also be calculated as:

$$k_{eff} = \sum_i \phi_i k_i \tag{4}$$

where the thermal conductivity of each constituent is denoted by k_i [43,54]. While this configuration corresponds to anisotropic heat transfer perpendicular to the heat source, other methods of calculating transport properties can be applied to other configurations. For example, microencapsulated PCM structures [55] would represent systems with highly isotropic heat transfer from which transport properties could be determined using the calculation described by Hashin and Shtrikman [56] and alternatively referred to as the Maxwell–Eucken bounds. Additionally, specific heat transfer models have been developed for alternating layers [54,57], and lattice structures [58,59], among others.

3.1.3. Quasi-steady state (QSS) approximation

In addition to the homogeneous composite approximation, the melting problem in composite systems can further be simplified using the quasi-steady state (QSS) approximation. This approximation assumes the conduction time through the liquid is short relative to the melt time. These assumed conditions lead to constant temperature gradients within the liquid phase ($\frac{\partial^2 T_l}{\partial y^2} = 0, \frac{\partial^2 T_l}{\partial r^2} = 0$), making the analytical melting problem more tractable [60-62]. This assumption is considered valid for very low Stefan numbers ($\text{St} \ll 1$), which implies the role of sensible heat is very small compared to the role of latent heat at the melt front interface [62-65]. Therefore, this approximation is most suitably applied for materials with very high latent heat values under low to moderate magnitude thermal loads, which is highly applicable for a large portion of PCM applications.

3.2. Approximate equations

In subsequent sections we establish the fundamental heat transfer equations which are used to develop an analytical optimization framework. More complete derivations described in the following sections are discussed in works by Hill [60] and Alexiades [61] among others.

3.2.1. Cartesian melting descriptions – Applied heat flux BC

We first consider the 1D cartesian melting problem with an applied constant heat flux boundary condition. We set the boundary at location, $y = 0$, which corresponds to the planar interface between the heat source and the PCM composite layer. Heat flows in the positive y direction away from this source. Using the QSS approximation, the increase in temperature at the heated boundary, $\Delta T_0 = T(y = 0) - T_m$, is:

$$\Delta T_0(t) = \frac{q_0'' \delta(t)}{k_{eff}}, y = 0 \tag{5}$$

where q_0'' corresponds to the applied thermal heat flux at the boundary, k_{eff} corresponds to the effective thermal conductivity and $\delta(t)$ represents the location of the melt front as a function of time, which is given by:

$$\delta(t) = \frac{q_0'' t}{L_{\text{v,eff}}} \tag{6}$$

where $L_{\text{v,eff}}$ represents the effective volumetric latent heat of the composite. Combining Eqs. (5) and (6) yields the equation for the temperature rise at the heated boundary over the initial temperature of the material, ΔT_0, as a function of time:

$$\Delta T_0(\text{t}) = \frac{q_0''^2 t}{k_{\text{eff}} L_{\text{v,eff}}}, y = 0 \tag{7}$$

3.2.2. Cartesian melting descriptions – Applied constant temperature BC

For the complementary problem of an applied constant temperature boundary condition, at $y = 0$ the heat flux into the system through the heated boundary interface (q_0'') is given as:

$$q_0''(t) = k_{\text{l}} \frac{\Delta T_0}{\delta(t)}, \tag{8}$$

where ΔT_0 is the difference between the applied temperature of the heated boundary and the initial temperature set to T_{m} ($\Delta T_0 = T(y = 0) - T_{\text{m}}$). Additionally, the location of the melt front, $\delta(t)$, can be expressed as:

$$\delta(t) = \sqrt{\frac{2 k_{\text{eff}} \Delta T_0 t}{L_{\text{v}}}} \tag{9}$$

Substituting Eq. (9) into Eq. (8) allows for the expression of heat flux into the system in terms of boundary condition and material properties as a function of time:

$$q_0''(t) = \sqrt{\frac{L_{v,eff} k_{eff} \Delta T_0}{2t}}, y = 0 \tag{10}$$

3.2.3. Cylindrical melting descriptions – Applied heat flux BC

We assume approximately the same configuration to establish analogous equations for cylindrical systems with the boundary at location r_0, which corresponds to the cylindrical interface between the heat source

and the PCM composite heat sink. The heat flows through the composite in the r direction away from this source until reaching the outer boundary at r_f. For the boundary condition of an applied heat flux, the QSS solution the temperature rise at the inner radius boundary ($\Delta T_0 = T(r = r_0) - T_m$) can then be described as:

$$\Delta T_0(t) = -\frac{q_0'' r_0}{k_{eff}}\left\{ln\left(\frac{r_0}{\delta(t)}\right)\right\}, r = r_0 \tag{11}$$

where the melt front location $\delta(t)$ in the radial direction is given by:

$$\delta(t) = \sqrt{\frac{2q_0'' r_0 t}{L_{v,\text{eff}}} + {r_0}^2} \tag{12}$$

Combining Eqs. (11) and (12) yields the equation for temperature rise at the inner radius boundary as a function of time:

$$\Delta T_0(t) = \frac{q_0'' r_0}{k_{eff}}\left\{ln\left(\sqrt{\frac{2q_0'' t}{r_0 L_{v,eff}} + 1}\right)\right\}, r = r_0 \tag{13}$$

3.2.4. Cylindrical melting descriptions – Applied constant temperature BC

Lastly the necessary equation for Cylindrical based melting systems with an applied constant temperature boundary condition at the inner radius completes our analytical basis. The key equation for heat flux into the system through the inner radius heated boundary is expressed as:

$$q_0''(t) = -k_{eff}\frac{\Delta T_0}{r_0 ln(r_0/\delta(t))}, r = r_0 \tag{14}$$

Furthermore, the location of the melt front travelling radially through the system is given as:

$$\delta(t)(1 + ln(r_0/\delta(t))) = r_0 - \frac{k_{eff}\Delta T_0 t}{r_0 L_{v,eff}} \tag{15}$$

Due to the nature of the of the above location it is not possible to analytically isolate $\delta(t)$ but numerical methods can be used to further advance design capabilities.

3.3. Deriving optimums

To create expressions for an optimal volume fraction of components, it is first necessary to define the objective that we are designing for. For an applied heat flux boundary condition, we will be considering the design objectives of: minimizing T_0 at a given optimization time,t', (§ **3.3.1**) and maximizing the duration the heated boundary can stay below a given allowable temperature threshold, T_{thresh} (§ **3.3.2**). For an applied constant temperature boundary condition, we will be considering the design objectives of: maximizing q''_0 at a given optimization time,t', (§ **3.3.3**) and maximizing the duration the system can stay above a minimum allowable heat flux,q''_{thresh}, i.e., dissipating at least a given level of power (§ **3.3.4**). The collection of all these objectives and geometries allows for this work to be broadly applied to many common applications.

In the following sections we derive analytical expressions for optimal volume fraction. An expression is derived for every combination of coordinate basis (Cartesian/cylindrical), boundary condition (applied $\Delta T_0/q_o''$), and design objective. Furthermore, independent expressions are developed for the *rate limited* and *volume limited* regimes. In the *rate limited* regime, the volume fraction is selected based on the rate the material can absorb heat. In the *volume limited* regime, the volume fraction is selected based on the thermal capacitance limits. From the resulting volume fraction values for each regime, the lower volume fraction of the two will be the optimal design choice, as discussed in § **3.1.1**.

For the design objective of optimizing a specific performance metric at a given time (§ **3.3.1**, § **3.3.3**), in the *rate limited* regime the performance metric, determined by the given boundary condition, is maximized analytically with respect to volume fraction to identify the optimum. The optimum in the *volume limited* regime is identified such that PCM melting completes at the time under investigation to select for a more thermally capacitive competition, delaying the drop in performance associated with melting completion.

For the design objective of maximizing the time for achieving a given minimum level performance (§ **3.3.2,** § **3.3.4**), in the *rate limited* regime the allowable time is maximized analytically with respect to volume fraction to identify the optimum. The *volume limited* optimal volume fraction is obtained by an analytical balancing of rate of thermal absorption and thermal capacitance. This is achieved by selecting a volume fraction such that the time to complete PCM melting corresponds with the time the threshold of performance is met.

3.3.1. Boundary condition: Applied heat flux

$$\boldsymbol{q}''(\boldsymbol{y} = 0|\boldsymbol{r} = \boldsymbol{r_o}) = \boldsymbol{q_o''}$$

Objective function: Minimize the temperature at a given time

$$\textbf{min}(\boldsymbol{T}(\boldsymbol{y} = 0|\boldsymbol{r} = \boldsymbol{r_o}, \boldsymbol{t})) \textbf{ for } \boldsymbol{t} = \boldsymbol{t'}$$

Consider first the case of a constant defined heat flux, $q''(y = 0|r = r_o) = q_o''$, that will operate for a specific amount of time, with the goal of minimizing the temperature of the heated surface at a particular optimization time, $min(T(y = 0|r = r_o, t))$ for $t = t'$.

To optimize the system when in the *rate limited* regime for Cartesian based systems Eq. (7) is rewritten as a function of volume fraction:

$$\Delta T_0 = \frac{{q_0''}^2 t}{(k_{metal}(\phi) + k_{PCM}(1-\phi))L_{v,PCM}(1-\phi)} \tag{16}$$

where the minimum temperature rise corresponds to:

$$\phi_{OPT,cart} = \frac{(k_{metal} - 2k_{PCM})}{2(k_{metal} - k_{PCM})}. \tag{17}$$

Under the rate limited regime for this configuration, the optimal volume fraction is exclusively a function of the thermal conductivity of the constituent materials.

When pursuing the objective of minimizing the temperature at a given time for cylindrical based systems, the temperature rise at the inner radius, Eq. (13), can be minimized similarly.

$$(k_{metal}(\phi) + k_{PCM}(1-\phi))q_0'' r_0 t' - L_{v,PCM}(1-\phi)^2\left(\frac{2q_0'' r_0 t'}{L_{v,PCM}(1-\phi)} + {r_0}^2\right)(k_{metal} - k_{PCM})ln\left(\sqrt{\frac{2q_0'' t'}{L_{v,PCM} r_0 (1-\phi)} + 1}\right) = 0 \tag{18}$$

This equation can then be solved numerically to determine the volume fraction that will minimize the temperature of a given system with no edge effects at a given time. Unlike the Cartesian case, optimal volume fraction for cylindrical systems in the *rate limited* regime is dependent on time and geometry.

For a Cartesian system in the *volume limited* regime, the optimal volume fraction can be solved using Eq. (6) and setting the melt front location to the edge of the system ($\delta(t) = y_f$). Substituting in the effective property calculation for latent heat, and solving for volume fraction yields:

$$\phi_{OPT,cart} = 1 - \frac{q_0'' t'}{y_f L_{v,PCM}} \tag{19}$$

In this case the optimal volume fraction is determined by the height of the system, the latent heat, the heat flux load and the time at which the system is being optimized.

The same approach may be taken for *volume limited* cylindrical

systems, using Eq. (12) and setting the melt front location equal to the outer radius ($\delta(t) = r_f$). Substituting in the effective property calculation for latent heat, and solving for volume fraction yields:

$$\phi_{OPT,cyl} = 1 - \frac{2q_0'' r_0 t'}{L_{v,PCM}(r_f^2 - r_0^2)} \tag{20}$$

This expression follows the same form as the cartesian result (eq (19).) while accounting for radially varying thermal mass.

3.3.2. Boundary condition: Applied heat flux

$$\boldsymbol{q}''(\boldsymbol{y} = 0|\boldsymbol{r} = \boldsymbol{r_o}) = \boldsymbol{q_o''}$$

Objective function: Maximize the time to stay below a given threshold temperature

$$\textbf{max } (\textbf{t}) \textbf{ for } \boldsymbol{T}(\boldsymbol{y} = 0|\boldsymbol{r} = \boldsymbol{r_o}) \langle \boldsymbol{T_{\textbf{thresh}}}$$

For the next objective we can consider a power source that can be run up until a defined upper temperature limit is reached, T_{thresh}. It is crucial in this scenario to have a design method to prevent the overheating and damage to the power source component or surrounding system. This upper limit can also be defined as a temperature threshold:

$$\Delta T_{thresh} = T_{thresh} - T_{m,} \tag{21}$$

which cannot be exceeded.

For this objective, when the system is *rate limited*, the solution can be obtained simply through isolating the time component. Rearranging Eq. (7) for time and substituting in effective property calculations yields:

$$t = \frac{(k_{metal}(\phi) + k_{PCM}(1-\phi))L_{v,PCM}(1-\phi)\Delta T_0}{q_0''^2} \tag{22}$$

Maximizing this equation when $\Delta T_0 = \Delta T_{thresh}$, yields the same volume fraction as the previous Cartesian *rate limited* response described by Eq. (17). This is expected because the optimal volume fraction in the Cartesian coordinate system does not vary with time or melt front location.

The cylindrical *rate limited* case will differ between design objectives due to the time and geometric dependance of the melt front circumference and associated volume. For this regime, Eq. (13) can be taken and rearranged for time. Substituting the effective material properties for the latent heat and thermal conductivity, we attain the expression for heat a specific time as a function of volume fraction.

$$t = \frac{r_0 L_{v,PCM}(1-\phi)(e^{2\Delta T_0(k_{PCM}(1-\phi)+k_{metal}(\phi))/q_0'' r_0} - 1)}{2q_0''} \tag{23}$$

Maximizing Eq. (23) then yields the following optimal composition:

$$\phi_{OPT,cyl} = \frac{2\Delta T_{thresh}(k_{metal} - k_{PCM}) - q_0'' r_0}{2\Delta T_{thresh}(k_{metal} - k_{PCM})} \tag{24}$$

For Cartesian based systems, the limiting factor of thermal capacitance can be described using the time to complete melting, Eq. (6), with an effective latent heat calculation to get:

$$t = \frac{L_{v,PCM}(1-\phi)(y_f)}{q_0''} \tag{25}$$

This can then be substituted into Eq. (16), setting, $\Delta T_0 = \Delta T_{thresh}$ and simplified to get the optimal volume fraction of the *volume limited* regime as:

$$\phi_{OPT,cart} = \frac{y_f q_0'' - k_{PCM}(\Delta T_{thresh})}{\Delta T_{thresh}(k_{metal} - k_{PCM})} \tag{26}$$

The same approach from the Cartesian development can then be applied to Cylindrical based systems for the *volume limited* regime. Taking the equation for melt front location (Eq. (12)) and rearranging to get the time to complete melting yields:

$$t = \frac{(r_f^2 - r_0^2)L_{v,PCM}(1-\phi)}{2r_0 q_0''} \tag{27}$$

Substituting the time of melting completion from Eq. (27) into Eq. (13), setting, $\Delta T_0 = \Delta T_{thresh}$ and solving for volume fraction then results in the equation:

$$\phi_{OPT,cyl} = \frac{q_0'' r_0 \ ln(r_0/r_f) + \Delta T_{thresh} k_{PCM}}{\Delta T_{thresh}(k_{PCM} - k_{metal})} \tag{28}$$

3.3.3. Boundary condition: Applied constant temperature

$$\mathbf{T}\ (\boldsymbol{y} = 0|\boldsymbol{r} = \boldsymbol{r_o}) = \boldsymbol{T_o}$$

Objective function: Maximize the heat flux at a given time

$$\boldsymbol{max}(\boldsymbol{q}''(\boldsymbol{y} = 0|\boldsymbol{r} = \boldsymbol{r_o}, \boldsymbol{t})) \textbf{ for } \boldsymbol{t} = \boldsymbol{t}'$$

In addition to considering system with an applied heat flux, it is also useful to develop optimization of systems with an applied constant temperature boundary condition. An applied constant temperature boundary is most closely analogous to the cooling of a heat pipe with a roughly isothermal liquid circulating through the system. If it is known that there will be a thermal load for a given amount of time, it may be desirable to maximize the heat absorption up to a given time based on the thermal loads of the system.

Within this configuration, first we develop an optimization for Cartesian geometries in the *rate limited* regime. Using an effective properties substitution in Eq. (10) the heat flux into a Cartesian system is given by:

$$q_0'' = \sqrt{\frac{(k_{metal}(\phi) + k_{PCM}(1-\phi))(L_{v,PCM}(1-\phi))\Delta T_0}{2t}} \tag{29}$$

The maximization of this equation then yields the optimum described by Eq. (17), and is consistent across all *rate limited* solutions in Cartesian based systems.

The cylindrical system under an applied constant temperature boundary condition presents a much more challenging problem due to the transcendental nature of the solution for the melt front location. To optimize for this case a numerical method is used to test across all volume fractions for the composition that will yield the largest flux at the time of optimization using Eqs. (14) and (15).

In the applied constant temperature boundary condition case, the *volume limited* optimal volume fraction is calculated using the equation for melt front location (eq. (9)) and substituting in the effective latent heat and thermal conductivity:

$$y_f = \sqrt{\frac{2(\ k_{metal}(\phi) + \ k_{PCM}(1-\phi)\ )\Delta T_0 t}{L_{v,PCM}(1-\phi)}} \tag{30}$$

This equation can then be solved to identify the optimal volume fraction as:

$$\phi_{OPT,cart} = \frac{L_{v,PCM} y_f^2 \ - \ 2\ k_{PCM} t' \Delta T_0}{L_{v,PCM} y_f^2 + 2\ t' \Delta T_0 (k_{metal} - k_{PCM})} \tag{31}$$

Applying the same approach to the cylindrical case, Eq. (15) for the location of the melt front can be used with effective material properties substituted as follows:

$$\delta(t)(1 + ln(r_0/\delta(t))) = r_0 - \frac{(\ k_{metal}(\phi) + \ k_{PCM}(1-\phi)\ )\Delta T_0 t}{r_0\ L_{v,PCM}(1-\phi)} \tag{32}$$

This expression can then be solved, replacing $\delta(t)$ with the outer radius of the system r_f and solving for the volume fraction as:

$$\phi_{OPT,cyl} = \frac{r_f\ r_0\ L_{v,PCM}(1 + ln(r_0/r_f)) - \ L_{v,PCM} r_0^2 + k_{PCM} t'\ \Delta T_0}{r_f\ r_0\ L_{v,PCM}(1 + ln(r_0/r_f)) - \ L_{v,PCM} r_0^2 + t'\ \Delta T_0 (k_{PCM} - k_{metal})} \tag{33}$$

3.3.4. Boundary condition: Applied constant temperature

$$\mathbf{T}\ (y = 0|\boldsymbol{r} = \boldsymbol{r_o}) = \boldsymbol{T_o}$$

Objective function: Maximize the time to stay above a threshold heat flux

$$\mathbf{max}\ (\mathbf{t})\ \mathbf{for}\ \boldsymbol{q}''(y = 0|\boldsymbol{r} = \boldsymbol{r_o})\langle \boldsymbol{q}''_{\boldsymbol{thresh}}$$

The last objective we consider is to maximize the time (t) to stay above a threshold heat flux, q''_{thresh}, when an applied constant temperature boundary condition is applied. This can also be explained as ensuring the absorption of at least a certain level of heat for the longest amount of time. If an application seeks to operate components for as long as possible and the cooling components remain relatively isothermal the development below will be the most useful.

For the Cartesian case this can be calculated using Eq. (10) and rearranging to get:

$$t = \frac{(k_{metal}(\phi) + k_{PCM}(1-\phi))(L_{v,PCM}(1-\phi))\Delta T_0}{2q''^2_0} \tag{34}$$

Maximizing this equation with respect to volume fraction, when $q''_0 = q''_{thresh}$, yields Eq. (17) consistent once again across all *rate limited* Cartesian optimizations.

As previously discussed, analytical solutions for cylindrical systems under constant temperature loads are not apparent. Therefore, for the objective of maximizing the time of obtaining at least a given level of heat flux in the *rate limited* regime, we take a numerical approach. Testing across a sample space of volume fractions with corresponding effective properties, Eq. (14) can be used to determine the melt front location where the system would reach the heat flux threshold. This radius can then be substituted into Eq. (15) to calculate the corresponding time where the heated boundary would intersect with the chosen heat flux. From this the maximum time value can be taken and the corresponding volume fraction identified.

For the Cartesian case in the *volume limited* regime for the objective of staying above a minimum threshold heat flux into the system for the longest time, Eq. (9) can be used, rearranging for time:

$$t = \frac{y_f^2 L_{v,PCM}(1-\phi)}{2(\ k_{metal}(\phi) + \ k_{PCM}(1-\phi)\ )T_0} \tag{35}$$

Equation (10) can also be rearranged for time as follows:

$$t = \frac{(k_{metal}(\phi) + k_{PCM}(1-\phi))(L_{v,PCM}(1-\phi))\Delta T_0}{q''^2_0} \tag{36}$$

Equation (35) and (36) can then be set equal and simplified to get the optimal volume fraction of:

$$\phi_{OPT,cart} = \frac{q''_{thresh} y_f \ - k_{PCM}\Delta T_0}{\Delta T_0(k_{metal} - k_{PCM})} \tag{37}$$

which is a direct translation of Eq. (26), yielding the same form while utilizing different variables as boundary conditions.

To identify the equivalent result for the cylindrical system Eq. (14) can be used, substituting the thermal conductivity for an expression of effective properties:

$$q''_0 = -\ (k_{metal}(\phi) + k_{PCM}(1-\phi)\ )\frac{\Delta T_0}{r_0 ln(r_0/\delta(t)\ )} \tag{38}$$

The q''_0 value can then be assigned the minimum heat flux value given, q''_{thresh}, and the melt front location can be assigned to the outer radius ($\delta(t) = r_f$). The volume fraction can then be solved for as:

$$\phi_{OPT,cyl} = \frac{q''_{thresh} r_0 ln(r_0/r_f) + \Delta T_0 k_{PCM}}{\Delta T_0(k_{PCM} - k_{metal})} \tag{39}$$

3.4. Analytical summary

Table 2 summarizes the analytical framework derived in section 3.3, providing a guideline for optimal volume fraction selection across the different design objectives, limiting regimes, boundary conditions and coordinate systems.

4. Results and discussion

Throughout the following sections we assess the functionality and applicability of the above developed analytical models through comparison to numerical and experimental results from original work and examples from the existing literature. Temperature and heat flux values are chosen to generally reflect the thermal loads of low to moderate power thermal management systems.

4.1. Original experimental results

To create a practical comparison for the analytical model developed herein we experimentally compare systems with different volume fractions and observe how the optimal system changes over time. Using 3D printed aluminum three systems were printed with metal volume fractions of 0.3, 0.5, and 0.7 (Fig. 4b). Temperature is measured at the base of the structures. While higher volume fractions can achieve lower temperatures at shorter times, their lower composition of PCM causes them to melt faster, leaving the lower volume fractions to become the highest performing systems at longer times (Fig. 4c). This is consistent with the models and analysis contained in previous sections.

The analytical framework developed above is applied to an experimental dataset to assess the practical applicability of the models. In Fig. 4 we demonstrate the changes in predicted optimal volume fraction using the objective of minimizing temperature at a given time (Fig. 4a) or maximizing the time below a given temperature (Fig. 4d) for a set internal boundary condition of $7.3 Wcm^{-2}$. These can be directly compared to the experimental data showing the temperature of the different volume fraction systems over time (Fig. 4c). In all cases, the analytical model was able to predict the highest performing system out of the three tested.

For the optimization metric of minimizing the temperature at a given time, we select times of 76.4 s, 54.6 s, and 32.7 s after the onset of melting, which correspond with the volume fractions of 0.3, 0.5, and 0.7 (Fig. 4a). Because it is not possible to initialize the experiment isothermally exactly at the melting temperature, Eq. (20) is compensated with time (t) renormalized by the melting time ($t - t_m$) (Fig. 4a). This adds a new level of approximation to our analysis because the system does not isothermally heat from its starting temperature of 22 ℃ but is shown to minimally affect the accuracy of our models for this case. For each optimization time we accurately select the optimal performing composite composition out of the sample set which corresponds closely to the onset of edge effects, as expected, and predicted times corresponding with the completion of melting are correct to within approximately 10%.

For the optimization metric of maximizing the time below a given temperature, we select temperature thresholds of 46.3 ℃, 39.0 ℃, and 35.9 ℃, which correspond with the volume fractions of 0.3, 0.5, and 0.7 (Fig. 4d). These optimums are predicted by Eq. (28) and reveal that the experimentally measured temperature values seen here are lower than analytically predicted values, which is also confirmed by equivalent numerical testing using our finite element model. This discrepancy is primarily attributed to 1) temperature heterogeneities near the free surface where the temperature is measured due to heat loss to the surrounding environment, 2) the contribution of the thermal mass of the cartridge heater itself, as well as interfacial resistances between the heater and the base of the composite PCM, 3) shortcomings of the QSS-based solutions, which neglect the role of sensible heat, and 4) potentially minor convective effects which increase at lower volume fractions, longer times and higher temperatures. Regardless, the predicted

Table 2
Compilation of equations describing optimal volume fraction with various thermal configurations and objectives for PCM composites.

Cartesian

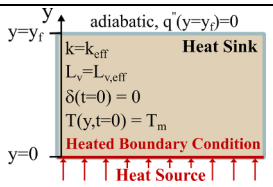

Heated Boundary Condition: Applied Heat Flux, $q''(y=0)=q_o''$
Objective Functions:
Minimize the temperature at a given time
Maximize the time to stay below a given threshold temperature

Objective Function	Rate Limited	Volume Limited
min $(T(y=0,t))$ for $t=t'$	$\phi_{cart}=\frac{(k_{metal}-2k_{PCM})}{2(k_{metal}-k_{PCM})}$ equation 17, § 3.3.1	$\phi_{cart}=1-\frac{q_0''t'}{y_f L_{v,PCM}}$ equation 19, § 3.3.1
max (t) for $T(y=0)<T_{thresh}$	$\phi_{cart}=\frac{(k_{metal}-2k_{PCM})}{2(k_{metal}-k_{PCM})}$ equation 17, § 3.3.2	$\phi_{cart}=\frac{y_f q_0''-\Delta T_{thresh}k_{PCM}}{\Delta T_{thresh}(k_{metal}-k_{PCM})}$ equation 26, § 3.3.2

Heated Boundary Condition: Applied Temperature, $T(y=0)=T_o$
Objective Functions:
Maximize the heat flux at a given time
Maximize the time to stay above a threshold heat flux

Objective Function	Rate Limited	Volume Limited
max $(q''(y=0,t))$ for $t=t'$	$\phi_{cart}=\frac{(k_{metal}-2k_{PCM})}{2(k_{metal}-k_{PCM})}$ equation 17, § 3.3.3	$\phi_{cart}=\frac{L_{v,PCM}y_f^2-2k_{PCM}t'\Delta T_0}{L_{v,PCM}y_f^2+2t'\Delta T_0(k_{metal}-k_{PCM})}$ equation 31, § 3.3.3
max (t) for $q''(y=0)<q''_{thresh}$	$\phi_{cart}=\frac{(k_{metal}-2k_{PCM})}{2(k_{metal}-k_{PCM})}$ equation 17, § 3.3.4	$\phi_{cart}=\frac{q''_{thresh}y_f-k_{PCM}\Delta T_0}{\Delta T_0(k_{metal}-k_{PCM})}$ equation 37, § 3.3.4

Cylindrical

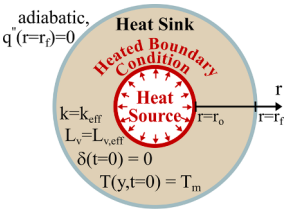

Heated Boundary Condition: Applied Heat Flux, $q''(r=r_o)=q_o''$
Objective Functions:
Minimize the temperature at a given time
Maximize the time to stay below a given threshold temperature

Objective Function	Rate Limited	Volume Limited
min $(T(r=r_o,t))$ for $t=t'$	Solve Equation 18 numerically equation 18, § 3.3.1	$\phi_{cyl}=1-\frac{2q_0''r_0t'}{L_v(r_f^2-r_0^2)}$ equation 20, § 3.3.1
max (t) for $T(r=r_o)<T_{thresh}$	$\phi_{cyl}=\frac{2\Delta T_{thresh}(k_{metal}-k_{PCM})-q_0''r_0}{2\Delta T_{thresh}(k_{metal}-k_{PCM})}$ equation 24, § 3.3.2	$\phi_{cyl}=\frac{q_0''r_0\ln(r_0/r_f)+\Delta T_{thresh}k_{PCM}}{\Delta T_{thresh}(k_{PCM}-k_{metal})}$ equation 28, § 3.3.2

Heated Boundary Condition: Applied Temperature, $T(r=r_o)=T_o$
Objective Functions:
Maximize the heat flux at a given time
Maximize the time to stay above a threshold heat flux

Objective Function	Rate Limited	Volume Limited
max $(q''(r=r_o,t))$ for $t=t'$	Maximize equation 14 for q'' using equation 15 to calculate $\delta(t')$ equations 14/15, § 3.3.3	$\phi_{cyl}=\frac{r_f r_0 L_{v,PCM}(1+\ln(r_0/r_f))-L_{v,PCM}r_0^2+k_{PCM}t'\Delta T_0}{r_f r_0 L_{v,PCM}(1+\ln(r_0/r_f))-L_{v,PCM}r_0^2+t'\Delta T_0(k_{PCM}-k_{metal})}$ equation 33, § 3.3.3
max (t) for $q''(r=r_o)<q''_{thresh}$	Maximize equation 15 for t using equation 14 to calculate $\delta(t)$ when $q''(r=r_o)=q''_{thresh}$ equations 14/15, § 3.3.4	$\phi_{cyl}=\frac{q''_{thresh}r_0\ln(r_0/r_f)+\Delta T_0 k_{PCM}}{\Delta T_0(k_{PCM}-k_{metal})}$ equation 39, § 3.3.4

optimums still provide approximate guide for the true optimums here and the validity of optimization through this performance metric is further explored numerically and through experimental work in the existing literature in the sections below.

4.2. Numerical comparison

In addition to experimental results, the analytical trends described in this work can be validated through direct comparison to numerical simulations. Numerical methods are useful in their ability to control every aspect of the system, as well as gather large quantities of data when compared with experimental methods. We use a previously

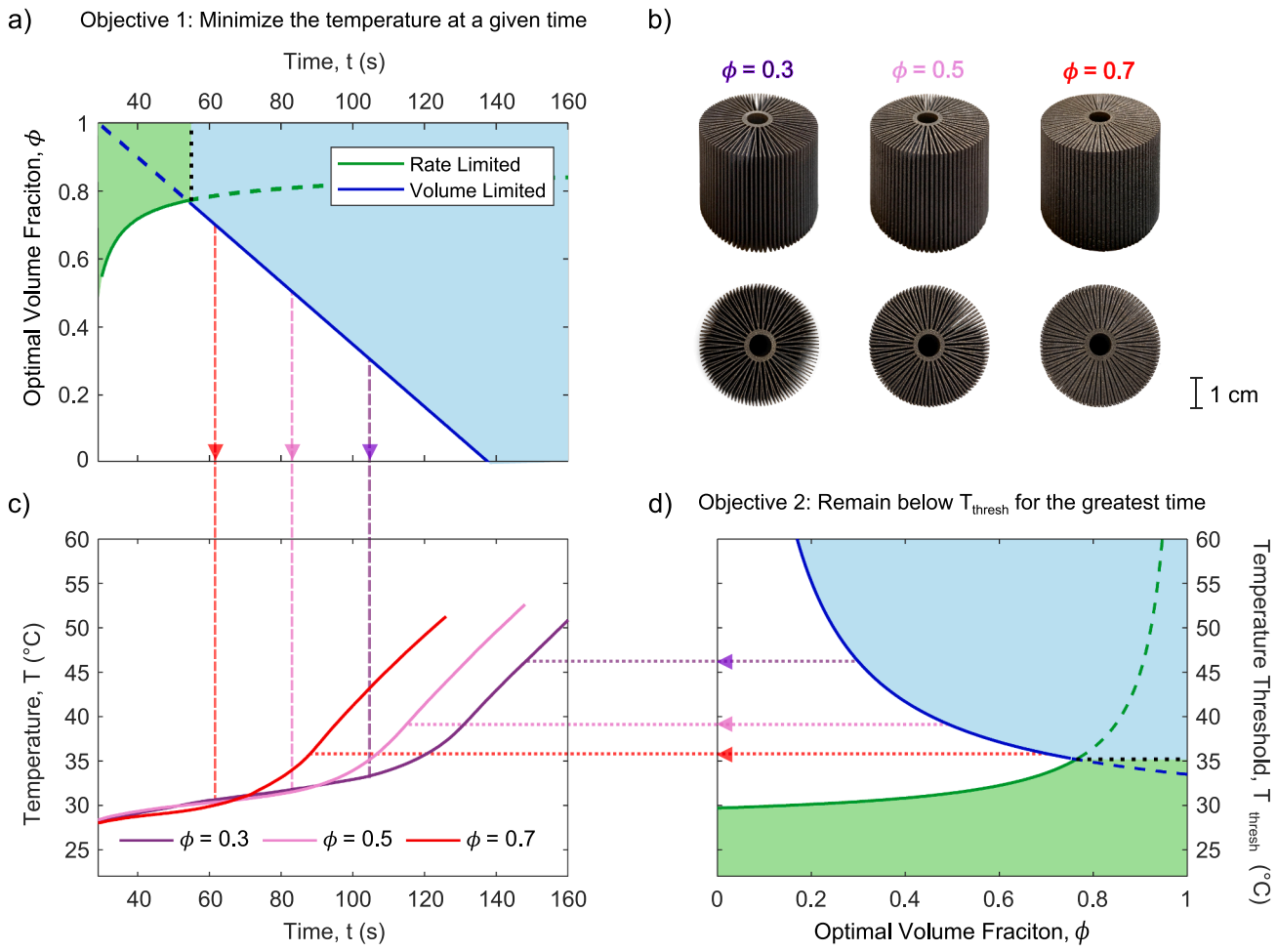

Fig. 4. Analytical results a) for the goal of minimizing the temperature at a given time the optimal volume fraction can be described over time. b) Photographs of the 3D printed physical aluminum systems for each of the volume fractions used in experimental results (0.3, 0.5, 0.7). Analytical results can be compared against c) experimental results for a Cylindrical finned heat sink under a heat flux load of 7.3 Wcm^{-2} $q''(r = r_o) = 7.3$ Wcm^{-2}, with volume fractions 0.3, 0.5, and 0.7. Analytical results d) for the goal of maximizing the time to stay below a given temperature the optimal volume fraction can be described for varying temperature increases. Dashed arrows indicate the relationship between the analytical results and behavior of the 3 tested structures.

established 1D finite difference model to test systems which employs the same homogenous composite approximation as our numerical development above [35,36,51].

4.2.1. Applied heat flux

Fig. 5 compares numerical and analytical optimization approaches for the given problem of optimizing a cylindrical system under a constant heat flux boundary condition. In our numerical methodology, the system is defined with a given composition and thermal load and continuously simulated until a given end condition is reached, defined as either reaching a given threshold temperature (Fig. 5a) or reaching a given time (Fig. 5b), depending on the design objective. The simulation basis is iterated to test a wide range of volume fractions in a short amount of time, for a cylindrical system thermal load of 6 Wcm^{-2}. There exists a clear pivot point in the volume fraction space which corresponds to the maximum value of the selected performance metric (Fig. 5a,b). Through a comparison to full simulation runs (Fig. 5c) it is evident that these optimums correspond to the point at which the PCM melting completes.

The predictions of the analytical model can be directly compared to the results given by the numerical model (Fig. 5a,b). For the cases shown here the analytical solution predicts results in the *volume limited* regime which is expected since the full simulation results show the optimum is related to the completion of melting. Asterisks are used in Fig. 5a-b to denote predicted analytical optimums calculated by Eq. (28) (Fig. 5a) and Eq. (20) (Fig. 5b). We observe that for either design objective the model is in strong alignment with the exhaustive results, demonstrating the accuracy of the model while highlighting the benefit of significantly reduced computational expense. It was also discovered that the models predicting optimal volume fraction for the goal of keeping the boundary temperature below a given threshold were more accurate than models created for the goal of minimizing temperature at a given time. This effect originates from the difference in time between the melt front reaching the outer boundary of the systems and completely melting the system, causing the true optimum to occur at the latter instance.

4.2.2. Applied constant temperature

Fig. 6 compares numerical and analytical optimization methodologies for the analogous problem of optimizing a cylindrical system under a constant temperature thermal load. For this boundary condition, the numerical simulation is run until the end condition of either falling below a threshold level of heat removal performance (Fig. 6a) or reaching a given time (Fig. 6b), depending on the design objective. For a cylindrical system thermal load of 29 °C, it can again be observed that there exists a clear pivot point in the volume fraction space which corresponds to the optimum of the performance being selected for (Fig. 6a, b). In the same fashion as the constant power boundary condition a comparison to full simulation runs (Fig. 6c) shows that these optimums

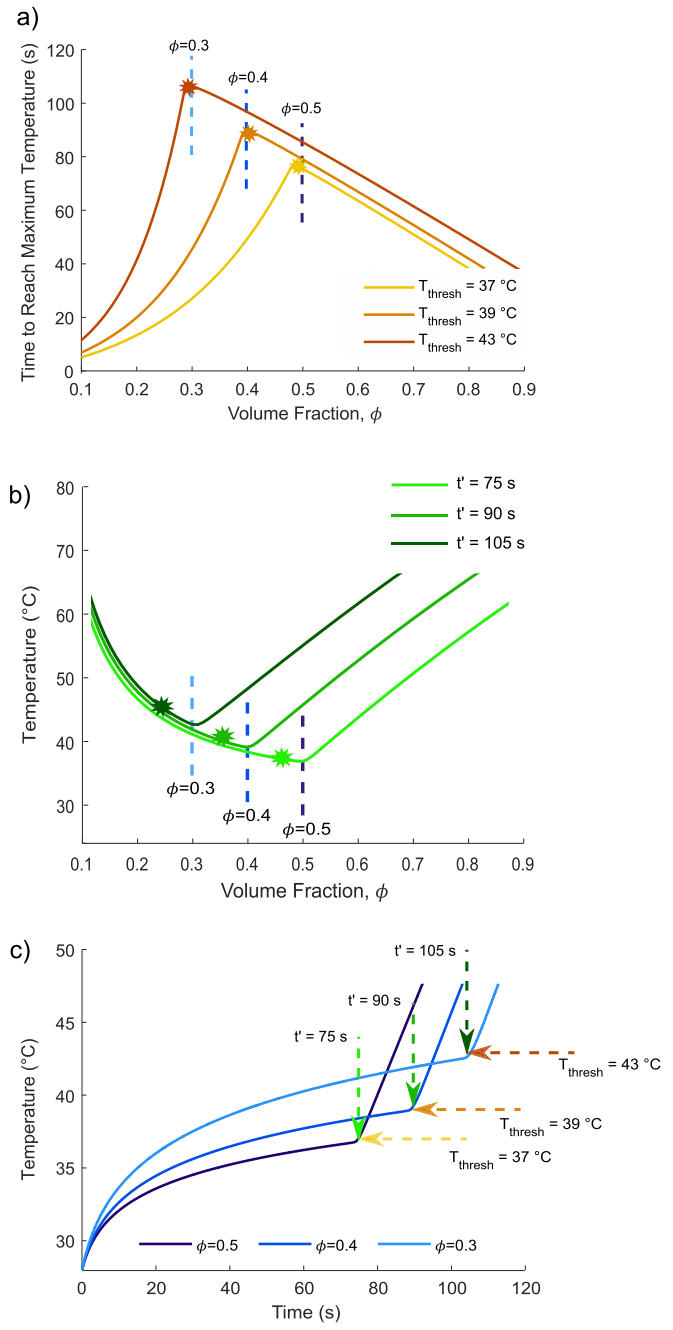

Fig. 5. For a cylindrical system thermal load of 6 Wcm^{-2} we present numerical results detailing the relationship between material compositions to a) the time at which PCM composites will reach the threshold temperature and b) the final boundary temperature at a given time. a,b) Volume fractions 0.3, 0.4, and 0.5 are denoted and asterisks indicate the optimal volume fractions predicted by analytical models above for each given end condition. c) Full simulation numerical results for a system under a thermal load of $q''(r = r_o) = 6\ Wcm^{-2}$, with 75 s, 90 s, 105 s denoting the times at which we are optimizing to minimize temperature and 37 °C, 39 °C and 43 °C denoting defined threshold temperatures which we wish to stay below for the longest amount of time.

correspond to the point at which the PCM melting completes, indicating that the application parameters fall within the *volume limited* regime. Asterisks are used in Fig. 5a-b to denote predicted analytical optimums calculated by Eq. (39) (Fig. 6a) and Eq. (33) (Fig. 6b), where we observe strong agreement between predicted and numerically determined optimums.

Comparison between analytical and numerical results contained in

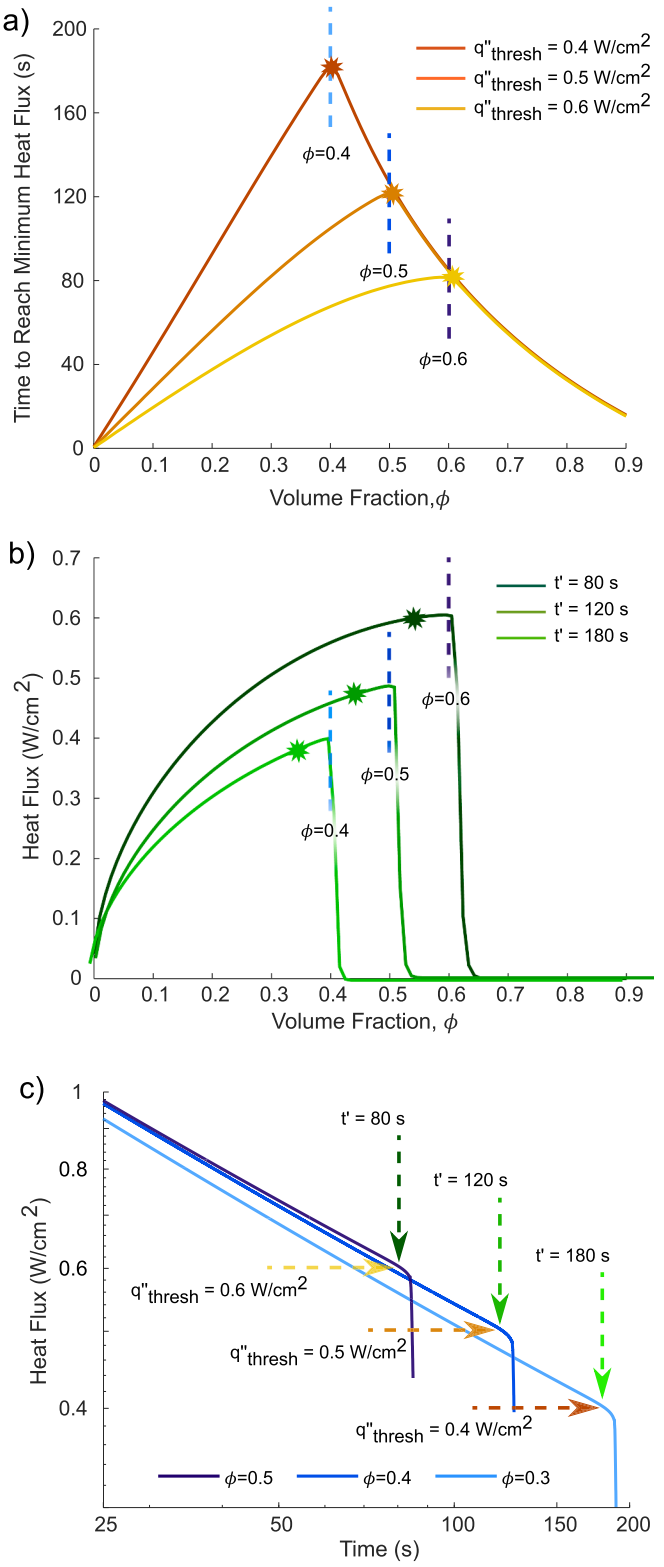

Fig. 6. For a cylindrical system thermal load of 29 °C we present numerical results detailing the relationship between material compositions to a) the time at which composites will reach the set threshold heat flux and b) the final boundary heat flux at a given time. a,b) Volume fractions 0.4, 0.5, and 0.6 are denoted and asterisks indicate the optimal volume fractions predicted by analytical models above for each given end condition. c) Full simulation numerical results for a system under a thermal load of $T(r = r_o) = 29^{\circ}C$, with 80 s, 120 s, 180 s denoting the times at which we are optimizing to maximize heat flux and 0.4 Wcm^{-2}, 0.5 Wcm^{-2} and 0.6 Wcm^{-2} denoting defined threshold heat fluxes which we wish to stay above for the longest amount of time.

Fig. 6 represents a very low magnitude boundary condition (29 °C) compared to the melting temperature (28 °C). This decision was made to demonstrate a more accurate portion of the parameter space. As was the case for the constant heat flux boundary condition, higher magnitude boundary conditions and longer times will decrease the accuracy of the model. Similarly, to the constant power case, the goal of maximizing the heat absorbed at a given time does not perfectly predict the numerical optimum (Fig. 6b). In contrast, the goal of maximizing the time the system is achieving at least a given minimum threshold heat flux leads to higher accuracy predictions, which is attributed to the time needed to melt the entirety of the outer radius simulated node.

4.2.3. Applicability range

As discussed in previous sections the accuracy of the models developed in this paper is highly dependent on the desired parameters of the application and originates largely a result of selecting the QSS solution for melting as an analytical basis. Therefore, it is necessary to explore the limits of the applicability of these models to understand how they may be applied to real systems. When comparing numerically observed and analytically predicted results we calculate high R^2 values indicating high predictive performance. Dividing our analysis between regimes using analytical predictions leads to coefficients of determination with consistent values of $R^2 \approx 1$ within the *rate limited* regime and an average of $R^2 \approx 0.93$ within the *volume limited* regime.

For the objective of minimizing temperature at a given time, the *rate limited* regime yields very high-fidelity predictions while the *volume limited* regime is the least accurate of the prediction regions studied here. Calculations of coefficients of determination show that the cylindrical results within this regime are the least accurate with $R^2 \approx 0.76$, compared to the Cartesian results with $R^2 \approx 0.97$, although the narrower range of inquiry within the Cartesian testing can contribute to this observation. Within the *volume limited* regime, our predictions align very strongly with numerical predictions at lower magnitudes of thermal loading but deviate with increased boundary condition magnitude (Fig. 7a). This is to be expected as the QSS solution is most valid when the role of sensible heat is small compared to the role of latent heat and will become less valid at longer times and higher thermal load. The deviation effects of the boundary magnitude are shown for a singular optimization time and will deviate more at longer times and have higher agreement at shorter times. It can be inferred from these results that, at high heat fluxes, if the model predicts a very low volume fraction in the *volume limited* regime, an offset towards higher volume fractions should be considered.

For the objective of maximizing the time below a given temperature, the accuracy of the model is shown to be much less dependent on operating parameters (Fig. 7b). In the *volume limited* regime both coordinate basis system classifications show extremely high agreement. In the *rate limited* regime, for both the Cartesian and cylindrical based systems, the analytical models slightly underpredicts the numerically predicted optimum but this is held relatively constant with varying optimization parameters. For this objective, coefficients of determination are found to have consistent values of $R^2 \approx 1$.

4.3. Application to previously reported experiments

4.3.1. Critical evaluation of numerical simulations

In addition to testing our analytical optimization against the original experimental and numerical data presented above, we are also able to draw on the existing literature to verify that our predictions are widely applicable. A 2015 study by Pakrouh et al. represents a quintessential study within the current PCM composite design space wherein different design configurations are used to empirically assess trends in performance [41]. This study employed a 3D computational fluid dynamics (CFD) model to simulate heat transfer through PCM based pin fin composite heatsinks under a thermal load of 1.02 W/cm^2, where the distribution of fins is uniform and rectilinear.

One of the most significant advantages to comparing our optimization methodology to existing datasets is to further justify the assumptions and approximations used throughout the development of this work. The CFD employed in the Pakrouh study diverges in the fundamental assumptions from the analytical and numerical models in this work in several ways, such as, 1) We approximate a macroscopic finned system as a 1D uniform composite which contrasts with the full 3D simulations executed in the Pakrouh study, 2) which also includes a metal base that we exclude. 3) The 3D simulation is initialized at a uniform temperature of 27 °C, while our models assume a uniform temperature distribution at the melting temperature starting from the solid state, which is compensated by the time to start melting in our following analysis. 4) Furthermore, in our work we assume a finite, well-defined, melting temperature while the PCM used in the Pakrouh study melts over a 5 °C range, from which we select the lowest value for our direct comparisons. 5) Finally, the CFD directly investigates the role of convection which is not included in our models. Consistent with previous literature and our claims, smaller spacing of fins led to minimal levels of convection even in the late stages of melting. Considering the sum of all these differences, our ability to predict optimal performances within the context of this work can greatly increase the confidence in our optimization methodology

For this paper we test the performance metric of optimizing performance, corresponding to minimizing temperature, at a given time. For the given materials, aluminum, and the commercial paraffin RT44 HC ($T_m = 41$–45 °C), the rate limited optimum would be $\phi = 0.5$ (Eq. (17)), which is not sampled at within the dataset. Consequently, we can

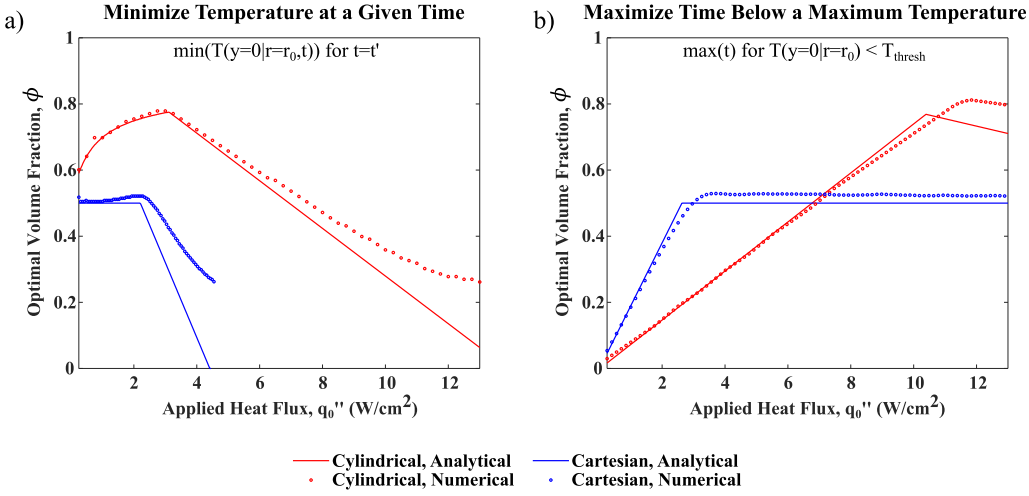

Fig. 7. Optimal volume fraction given by numerical results (dotted points) and analytical predictions (solid lines) in cylindrical (red) and Cartesian (blue) based systems a) for the objective of minimizing temperature at 60 s ($t' = 60s$) after thermal load onset and b) maximizing the time below a maximum threshold temperature of 38 °C ($T_{thresh} = 38\,°C$) for a system under varying thermal loads in. (For interpretation of the references to colour in this figure legend, the reader is referred to the web version of this article.)

analyze the lower volume fractions as optimal systems for different times and, while the highest of these volume fractions ($\phi = 0.73$) will never be optimal, applying the solution for the volume limited regime still allows us to assess the applicability of the equations and assumptions we are working with. For the shorter fin height, 15 mm, we propose the optimization times of 80 s, 190 s, and 240 s after the beginning of melting, which corresponds to the optimal volume fractions of 0.73, 0.35 and 0.18 (Eq. (19), Fig. 8a). For the 23 mm extended fin systems, we propose the optimization times of 140 s, 300 s, and 400 s after the beginning of melting which correspond to optimal metal volume fractions of 0.71, 0.38 and 0.18 (Eq. (19), Fig. 8b). For each of the optimization times selected, it is evident that the selected volume fraction yields the lowest temperature out of the three related volume fraction systems (Fig. 8). Furthermore, we confirm the optimality of the pivot point corresponding to the completion of melting as well as our ability to predict when it will occur. Our prediction is especially strong at the high volume fractions, which is explainable by the relationship between the increasing distance between fins, ranging from 1 mm to 8 mm, and the role of convection. Even at the lowest volume fractions where convection is certainly playing a role, we are still able to accurately select an optimal volume fraction and predict the approximate time of melting completion.

4.3.2. Critical evaluation of experimental observations

Another selection from the existing literature that can be used to directly asses the applicability of our optimization methodology is work by Tamraparni et al. from 2021 which sought optimal designs of lamellar PCM composites primarily using numerical and experimental methods [36]. The experimental aspects of this work serve as a useful validation of the real-world validation of the methodology we have developed. This work is especially useful because it represents one of the more complete experimental datasets within the literature and a thorough examination of different volume fraction systems under various heat flux conditions can be found in the supplemental information of this work (Fig. 9).

Using Eq. (17), a rate limited optimal volume fraction can be calculated as 0.5, which can clearly be observed as the highest performing composition across thermal loads and performance metrics throughout the study. Therefore, any volume fractions higher than this value can be rejected as possible optimums, which is confirmed within a reasonable level of randomness. For further analysis we consider the performance metric of maximizing the time the heated boundary can stay below a given maximum value in the volume limited regime. For the lowest power dataset, 1.45 W cm^{-2}, we propose temperature thresholds of 35 °C, 37 °C, and 40 °C which correspond to a predicted optimal composition of 0.43, 0.3 and 0.21 vol fraction of metal respectively (Eq. (26), Fig. 9a). As the heat flux is increased, the lowest volume fractions fall out of our analysis frame. Therefore, we propose two temperature thresholds for the 4.8 W cm^{-2} dataset of 48 °C, and 54 °C which correspond to a predicted optimal composition of 0.4 and 0.3 vol fraction of metal respectively (Eq. (26), Fig. 9b). Lastly, for the 7.25 W cm^{-2} dataset we select a temperature threshold of 57 °C which corresponds to a predicted optimal composition of 0.42 vol fraction of metal (Eq. (26), Fig. 9c). In all cases tested, our optimization methodology is able to select the volume fraction within the given sample range that maintains sub-threshold temperatures for the longest amount of time. Notably, we do not observe a decrease in accuracy with increasing levels of thermal loading, which increases our confidence in the quasi-steady state assumption used in our optimization methodology within a reasonable range of power levels.

4.4. Trends in optimums

To help understand how optimal volume fraction is dependent on application needs we can compare analytically optimized volume fraction selections across varying thermal loads. In Fig. 10 we map out an optimal composition space with varying parameters of the design problem. The geometric basis of the cylindrical design problem was chosen to mirror our experimental analysis with a 3.6 mm inner radius and outer radius of 19.1 mm, while the dimension associated with the Cartesian problem was chosen as 15.5 mm to match the width of the cylindrical composite layer. Simulated material properties are set as the known properties of octadecane and AlSi12 (Table 1).

Analysis of trends within the design space is particularly useful if the application parameters are not ideally set and may vary somewhat in thermal loading or run time. For such cases, an optimal composition can be identified, and knowledge of trends can be used to inform adjustments from said optimum. Fig. 10 demonstrates that the *rate limited* and *volume limited* regimes have very distinct trends over the analyzed space.

Notably, the optimum for systems with a Cartesian basis the optimal volume fraction in the *rate limited* regime is the same across all applications and design objectives because the solution is solely determined by material properties. Aside from this case, the optimal volume fraction will always decrease farther from the intersection of the two regimes. For cylindrical systems, the optimal volume fraction in the *rate limited* regime increases leading up to the regime intersection. This difference between cylindrical and Cartesian based systems can be attributed to an increase in circumferential thermal capacitance with increasing melt front propagation radius for cylindrical based systems compared to Cartesian based systems. This varying optimal volume fraction within

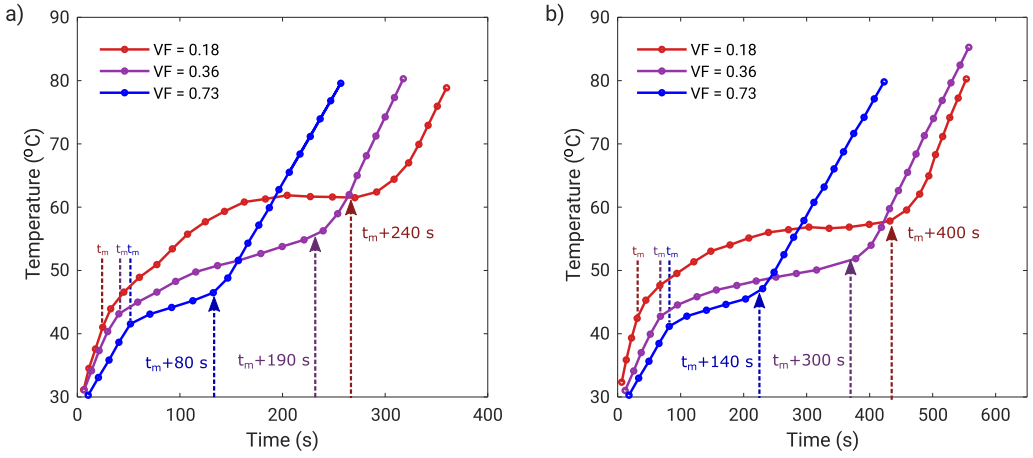

Fig. 8. Base temperature evolution with time for metal volume fractions of 0.18, 0.36 and 0.73 with a fin height of (a) 15 mm and (b) 25 mm. Dashed lines labeled with tm indicate the datapoint corresponding to the start of melting when the lowest temperature of the melting range is reached, and dashed arrows indicate optimization times that correspond to the given compositions (within 3 %) when pre-selecting a volume limited solution. Modified from Pakrouh et al, 2015 [35].

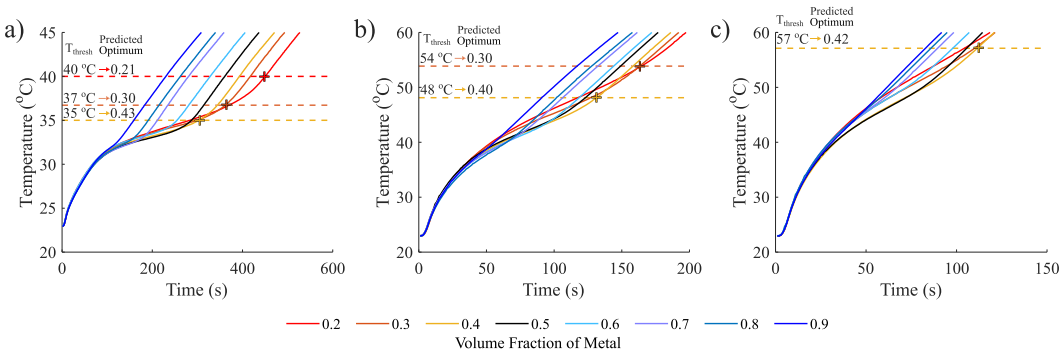

Fig. 9. Temperature vs time plots systems for Cartesian based octadecane and aluminum alloy composites with varying volume fraction of metal for heat flux boundary conditions of (a) 1.45 W cm^{-2}, (b) 4.8 W cm^{-2} and (c) 7.25 W cm^{-2}. Dashed horizontal lines indicate a temperature threshold and are labeled with the volume fraction predicted to satisfy the optimization of maximizing the time to stay below the threshold. Modified with permission from Tamraparni et al, 2021 [36].

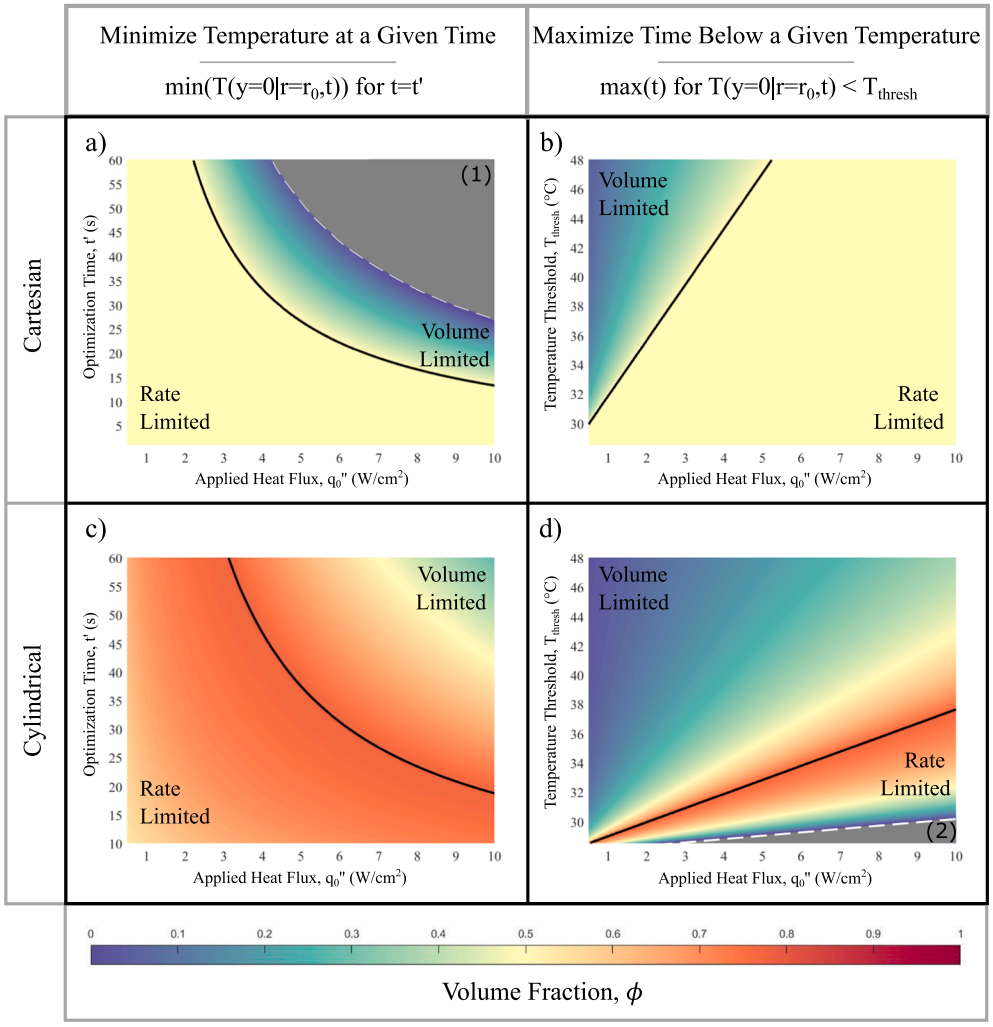

Fig. 10. Example maps of optimal volume fraction with varying thermal inputs for a,b) Cartesian systems and c,d) cylindrical systems with a,c) the goal of minimizing the temperature at different times ($min(T(y=0|r=r_o,t))$ for $t=t'$) and b,d) the goal of maximizing the time the system's heated boundary can remain below a range of threshold temperatures (max(t) for $T(y=0|r=r_o,t)\langle T_{thresh}$), for varying thermal loads. Black solid lines indicate the divide between the rate limited regime and the volume limited regime. Dashed white lines indicate the border of the region where optimization is bounded, where (1) the PCM volume is insufficient to manage the thermal load and (2) the problem is ill defined due to extremely short time scales.

the rate limited regime for cylindrical systems suggests that while a completely uniform material is the optimal configuration for Cartesian systems, compositionally variant systems present an opportunity for future work in cylindrical systems.

For all cases in the *volume limited* regime, the optimal volume fraction will always decrease with distance from the regime boundary intersection. This can be rationalized as a necessity to increase the time before the completion of melting. This is expected by recalling the completion of melting corresponds to a sharp decrease in performance and the addition of thermal capacitance will delay the onset of this point.

We also identify regimes indicated by the gray regions in Fig. 10, where the analytical model yields solutions less than zero (Fig. 10a,d). In this regime having a completely PCM system is the optimal composition, assuming a PCM based solution, but using a PCM is likely not the ideal thermal management approach if all other design problem parameters are fixed. This is because, in these cases, the dynamics of the melting process begin to be dwarfed by the thermal loading making the temperature damping from the phase change process insignificant. There

are two explanations for these bounds which are unique to the corresponding framing of the optimization problem. When considering the problem of minimizing the temperature at a given time, the optimization is bounded in the *volume limited* regime in the limits of longer time and applied heat flux (Fig. 10a, grey region). This can be understood as the conditions under which the system volume is insufficient for the application and even a complete PCM composition cannot prevent the completion of melting, after which performance rapidly drops off. When considering the problem of maximizing the time the system can remain below a given temperature, a different bound emerges (Fig. 10d, grey region). This bound can be understood as the region where the problem is ill defined, i.e. in this region the time to reach the threshold temperature is very small (~1 s) and the difference between differing compositions becomes negligible.

4.5. Example optimization processes

In this section we provide practical examples of the application of this work. We constrain the problem to only consider optimization with aluminum and octadecane with properties defined in Table 1. In each example we assume the initial state of the material system is entirely solid and held at a negligible distance from the melting temperature. All edges of the system, aside from the heated boundary, are considered adiabatic. Solutions to thermal problems below are assumed to be in the form of finned heatsinks, representing the upper limit of anisotropic heat transfer away from the heat source [43]. Furthermore, fin spacings are assumed to be sufficiently small to achieve homogeneous composite behavior [35-37].

Example Problem 1:

Consider a cylindrical battery producing heat at a rate of $q_0'' = 10\ Wcm^{-2}$ nested in a concentric cylindrical thermal storage package with an allowable inner radius of $r_o = 0.5cm$ and outer radius of $r_f = 2cm$. The goal of this thermal storage package is to keep the temperature of the battery below 48 ℃ (i.e. 20 ℃ over the melting temperature, $\Delta T_{thresh} = 20°C$) for the longest possible amount of time.

The *rate limited* solution to this problem is solved using Eq. (24) yielding a volume fraction of $\phi = 0.84$. The *volume limited* solution to this problem is solved using Eq. (28) yielding a volume fraction of $\phi = 0.43$. Per our methodology the lower of the two values is the true optimum, which is $\phi = 0.43$, indicating we are in the *volume limited* regime of the design problem.

To support this optimization result and demonstrate the disadvantages of deviating from the optimal composition, we employ our numerical model to simulate various compositions within the design space and asses the timescales associated with each composition for the given temperature threshold (Fig. 11). At the optimal volume fraction, the battery surface can remain below the threshold temperature for ~ 43 s (Fig. 11a). For this particular design problem, if the system is PCM deficient, i.e. the volume fraction is higher than the optimum, the performance as measured by the time below the threshold temperature decreases linearly by ~ 12% of the optimum for every increment of 10% of the sample space range ($\phi = 0.1$) (Fig. 11b). If the system is PCM rich, i.e. the volume fraction is lower than the optimum, the performance decreases more rapidly than the PCM deficient side of the problem. Within the first volume fraction increment of 10% ($\phi = \phi_{OPT} - 0.1$) the performance drops by ~ 40% and further steps drop quadratically with the fourth step corresponding to a performance drop of ~ 97% (Fig. 11b).

Example Problem 2:

As another example, consider an electronics chip producing heat at a level of $q_0'' = 1\ Wcm^{-2}$ attached to a rectangular thermal storage package with a maximum height given as $y_f = 1.5cm$. The design objective of the thermal storage package is to minimize the temperature of the chip over the time the chip is active, given as $t' = 120\ s$

The *rate limited* solution to this problem is solved using Eq. (17) yielding a volume fraction of $\phi = 0.50$. The *volume limited* solution to this problem is solved using Eq. (19) yielding a volume fraction of $\phi = 0.54$. Per our methodology the lower of the two values is the true optimum, which is $\phi = 0.50$, indicating we are in the *rate limited* regime of the design problem.

To support this optimization result and demonstrate the disadvantages of deviating from the optimal composition, we employ our numerical model to simulate various compositions within the design space and assess temperature associated with each composition at the optimization time (Fig. 12). At the optimal volume fraction, the chip surface at the optimization time reaches a temperature of 31 °C (Fig. 12a). For this particular design problem, if the system is PCM deficient, i.e. the volume fraction is higher than the optimum, the chip's surface temperature increases linearly by ~ 20% of the optimum for every increment of 10% of the sample space range ($\phi = 0.1$) (Fig. 12b). If the system is PCM rich, i.e. the volume fraction is lower than the optimum, the chip temperature is lower than the PCM deficient side of the problem. Within the first volume fraction increment of 5% ($\phi = \phi_{OPT} - 0.05$) the temperature deviates from the optimum by ~ 2% and further steps of the same increment approximately double with the furthest deviation from the optimum corresponding to a ~ 39% increase in temperature (Fig. 12b).

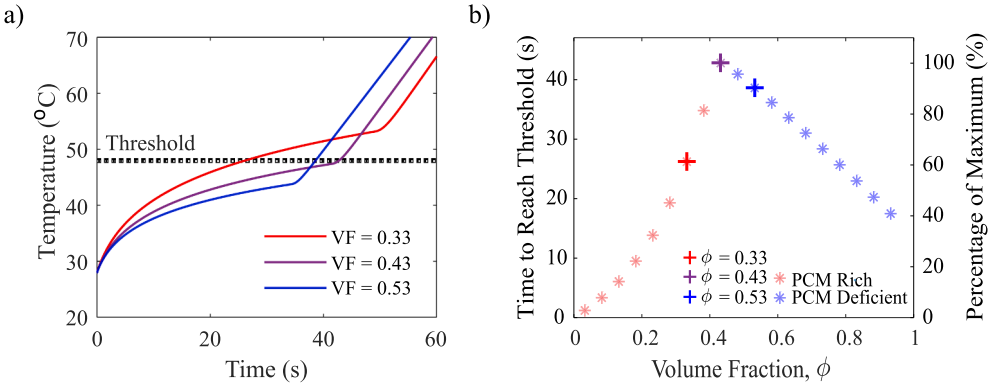

Fig. 11. a) Numerical results for the temperature of the battery surface boundary for the optimized thermal storage package $\phi = 0.43$and with a deviation from this optimum by 10% of the sample space range ($\phi = 0.33$/ $\phi = 0.53$). Temperature threshold given by the design problem indicated with dotted line, $\Delta T_{thresh} = 20\ °C$. b) Comparison of the performance, measured in time to reach the temperature threshold and as a percentage of the maximum time.

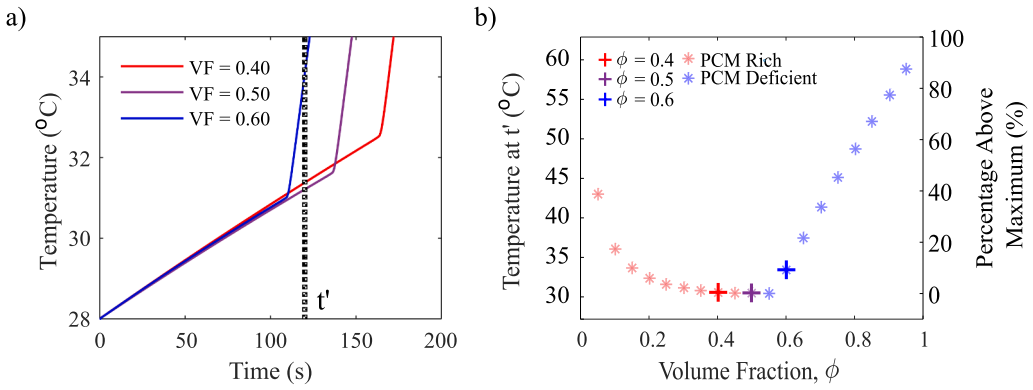

Fig. 12. a) Numerical results for the temperature of the battery surface boundary for the optimized thermal storage package $\phi = 0.5$ and with a deviation from this optimum by 10% of the sample space range ($\phi = 0.4/\ \phi = 0.6$). Optimization time given by the design problem indicated with dotted line, $t^{'} = 120\ s$. b) Comparison of the performance, measured in the temperature at the optimization time and as a percentage increase over the minimum temperature rise.

Lessons from examples

Working through specific examples allows us to identify common characteristics that are true of most practical cases, even if it is not a rule over the whole sample space. It has been observed over many test problems that when *rate limited* solutions are identified as the appropriate choice, especially when the *volume limited* optimum deviates from the *rate limited* optimum significantly, there is usually a large range of volume fractions with similar performances and deviating from the optimum often causes minimal decrease in thermal buffering capacity. This can be partially seen in Fig. 11 b where deviating from the optimum by $\phi = 0.05$ yields negligible changes in performance, though deviating farther causes melting to complete on the PCM deficient side. This is expected because the calculated *volume limited* solution is very close to the *rate limited* solution.

Within the *volume limited* regime, for the objective of maximizing thermal buffering at a given time, it is most commonly observed that, for equivalent deviations in volume fraction from the optimum, the PCM rich side of the design space decreases in performance at a lower rate than the PCM deficient side. In this regime, the complementary objective of maximizing the time to achieve a given minimum thermal buffering capacity usually exhibits a sharper peak in performance in the volume fraction space and any deviation from this optimum will cause significant decreases in performance without a strong preference for PCM deficiency or excess.

5. Conclusions

Phase change material based heat sink design is an area of intense interest in thermal management applications, wherein the composition of constituent elements remains the most critical design inquiry. In this manuscript, we establish a comprehensive analytical optimization framework for determining the compositions of constituent thermally conductive and capacitive components in composite phase change material layers for Cartesian and Cylindrical based systems. Within the design space, we describe two regimes where performance is limited by rate of heat absorption (*rate limited)* or total thermal capacitance (*volume limited)*, for which corresponding expressions are derived using the quasi-steady state approximation for melting problems. This design framework spans all permutations of 1) two coordinate bases 2) two boundary condition types and 3) two design objectives to allow for this work to be broadly applicable and practical to apply.

Through a comparison to exhaustive simulation-based optimization, we confirm the accuracy and usefulness of the developed analytical models, demonstrating consistent coefficients of determination of $R^2 \approx 1$ within the *rate limited* regime and an average of $R^2 \approx 0.93$ within the *volume limited* regime. When optimizing thermal buffering capacity in terms heat transfer through the system boundary, it is observed that analytical optimization models are most valid at lower power and shorter time scales as expected from the approximate models we use. We also demonstrate the practical applicability of this work through direct comparison to original experimental results as well as experimental and numerical results from the existing literature. The convergence between these high-fidelity simulations and experiments, and the approximate analytical framework outlined in this manuscript is remarkable and demonstrates the utility of this approach in generating high performing provisional designs of composite PCM structures. Example problems are used to demonstrate the application of this work, where we show an average of 14.6 % decrease in performance when deviating by only 10% of the composition range. In summary, his work provides an unprecedented degree of design control by providing practical and objective oriented guidelines for PCM composite design.

CRediT authorship contribution statement

Alison Hoe: Investigation, Methodology, Writing – original draft. **Michael T. Barako:** Conceptualization, Writing – review & editing. **Achutha Tamraparni:** Investigation. **Chen Zhang:** Investigation. **Alaa Elwany:** Supervision. **Jonathan R. Felts:** Writing – review & editing. **Patrick J. Shamberger:** Conceptualization, Supervision, Writing – review & editing.

Declaration of Competing Interest

The authors declare that they have no known competing financial interests or personal relationships that could have appeared to influence the work reported in this paper.

Acknowledgements

This material is based upon research supported by, or in part by, the U. S. Office of Naval Research under award number N00014-17-1-2802 with additional support from The National Science Foundation Research Traineeship Program grant 1545403.

References

[1] D. Hale, M. Hoover, and M. O'neill, "Phase change materials handbook," *National Aeronautics and Space Admnistration,* 1971.
[2] A. Sharma, V.V. Tyagi, C.R. Chen, D. Buddhi, Review on thermal energy storage with phase change materials and applications, Renew. Sustain. Energy Rev. 13 (2) (2009) 318–345.
[3] J. Stefan, Über die Theorie der Eisbildung, insbesondere über die Eisbildung im Polarmeere, Annalen der Physik und Chemie 278 (2) (1891) 269–286.
[4] J.C. Jaeger, H.S. Carslaw, Conduction of heat in solids, Clarendon Press, 1959.

[5] J. Crank, Free and moving boundary problems, Oxford University Press, USA, 1984.
[6] Y.A. Cengel, H. Pérez, Heat transfer: a practical approach., 2 ed., McGraw-Hill, 2002.
[7] D. Q. Kern and A. D. Kraus, "Extended surface heat transfer", 1972.
[8] P. J. Brennan and E. J. Kroliczek, "Heat Pipe Design Handbook: Volume II," *National Aeronautics and Space Admnistration,* 1979.
[9] E. Skrabek, "Heat pipe design handbook, part 1," *National Aeronautics and Space Admnistration,* 1972.
[10] D. Reay, R. McGlen, P. Kew, Heat pipes: theory, design and applications, Butterworth-Heinemann, 2013.
[11] K. Thulukkanam, Heat exchanger design handbook, CRC Press, 2013.
[12] K. Yazawa, P.J. Shamberger, T.S. Fisher, Ragone Relations for Thermal Energy Storage Technologies, Frontiers in Mechanical Engineering 5 (2019) 29.
[13] M.T. Barako, S. Lingamneni, J.S. Katz, T. Liu, K.E. Goodson, J. Tice, Optimizing the design of composite phase change materials for high thermal power density, J. Appl. Phys. 124 (14) (2018), 145103.
[14] P.J. Shamberger, T.S. Fisher, Cooling power and characteristic times of composite heatsinks and insulants, Int. J. Heat Mass Transf. 117 (2018) 1205–1215.
[15] J. Woods, A. Mahvi, A. Goyal, E. Kozubal, A. Odukomaiya, R. Jackson, Rate capability and Ragone plots for phase change thermal energy storage, Nat. Energy 6 (3) (2021) 295–302.
[16] T. Christen, Ragone plots and discharge efficiency-power relations of electric and thermal energy storage devices, J. Storage Mater. 27 (2020), 101084.
[17] J.M. Khodadadi, L. Fan, H. Babaei, Thermal conductivity enhancement of nanostructure-based colloidal suspensions utilized as phase change materials for thermal energy storage: A review, Renew. Sustain. Energy Rev. 24 (2013) 418–444.
[18] J.M. Khodadadi, S.F. Hosseinizadeh, Nanoparticle-enhanced phase change materials (NEPCM) with great potential for improved thermal energy storage, Int Commun Heat Mass 34 (5) (2007) 534–543.
[19] C.J. Ho, J.Y. Gao, Preparation and thermophysical properties of nanoparticle-in-paraffin emulsion as phase change material, Int Commun Heat Mass 36 (5) (2009) 467–470.
[20] M.A. Kibria, M.R. Anisur, M.H. Mahfuz, R. Saidur, I.H.S.C. Metselaar, A review on thermophysical properties of nanoparticle dispersed phase change materials, Energ Convers Manage 95 (2015) 69–89.
[21] Y. Guo, H. Yang, G. Lin, H. Jin, X. Shen, J. He, J. Miao, Thermal performance of a 3D printed lattice-structure heat sink packaging phase change material, Chin. J. Aeronaut. 34 (5) (2021) 373–385.
[22] G. Righetti, G. Savio, R. Meneghello, L. Doretti, S. Mancin, Experimental study of phase change material (PCM) embedded in 3D periodic structures realized via additive manufacturing, Int. J. Therm. Sci. 153 (2020), 106376.
[23] W.Q. Li, Z.G. Qu, Y.L. He, W.Q. Tao, Experimental and numerical studies on melting phase change heat transfer in open-cell metallic foams filled with paraffin, Appl. Therm. Eng. 37 (2012) 1–9.
[24] M. Iasiello, M. Mameli, S. Filippeschi, N. Bianco, Simulations of paraffine melting inside metal foams at different gravity levels with preliminary experimental validation, J. Phys. Conf. Ser. 1599 (1) (2020), 012008.
[25] A. Ghahremannezhad, H. Xu, M.R. Salimpour, P. Wang, K. Vafai, Thermal performance analysis of phase change materials (PCMs) embedded in gradient porous metal foams, Appl. Therm. Eng. 179 (2020), 115731.
[26] P.P. Levin, A. Shitzer, G. Hetsroni, Numerical optimization of a PCM-based heat sink with internal fins, Int. J. Heat Mass Transf. 61 (2013) 638–645.
[27] V. Shatikian, G. Ziskind, R. Letan, Numerical investigation of a PCM-based heat sink with internal fins, Int. J. Heat Mass Transf. 48 (17) (2005) 3689–3706.
[28] S. Mahmoud, A. Tang, C. Toh, R. Al-Dadah, S.L. Soo, Experimental investigation of inserts configurations and PCM type on the thermal performance of PCM based heat sinks, Appl. Energy 112 (2013) 1349–1356.
[29] Y. Huang, Q. Sun, F. Yao, C. Zhang, Experimental study on the thermal performance of a finned metal foam heat sink with phase change material, Heat Transfer Eng. 42 (7) (2021) 579–591.
[30] N. Bianco, S. Busiello, M. Iasiello, G.M. Mauro, Finned heat sinks with phase change materials and metal foams: Pareto optimization to address cost and operation time, Appl. Therm. Eng. 197 (2021), 117436.
[31] Z.A. Qureshi, E. Elnajjar, O. Al-Ketan, R.A. Al-Rub, S.B. Al-Omari, Heat transfer performance of a finned metal foam-phase change material (FMF-PCM) system incorporating triply periodic minimal surfaces (TPMS), Int. J. Heat Mass Transf. 170 (2021), 121001.
[32] J.M. Mahdi, E.C. Nsofor, Solidification enhancement of PCM in a triplex-tube thermal energy storage system with nanoparticles and fins, Appl. Energy 211 (2018) 975–986.
[33] I. Sarani, S. Payan, S. Nada, A. Payan, Numerical investigation of an innovative discontinuous distribution of fins for solidification rate enhancement in PCM with and without nanoparticles, Appl. Therm. Eng. 176 (2020), 115017.
[34] B. Kok, Examining effects of special heat transfer fins designed for the melting process of PCM and Nano-PCM, Appl. Therm. Eng. 170 (2020), 114989.
[35] A. Hoe, M. Deckard, A. Tamraparni, A. Elwany, J.R. Felts, P.J. Shamberger, Conductive heat transfer in lamellar phase change material composites, Appl. Therm. Eng. 178 (2020), 115553.
[36] A. Tamraparni, et al., Design and Optimization of Lamellar Phase Change Composites for Thermal Energy Storage, Adv. Eng. Mater. 23 (1) (2021) 2001052.
[37] T. Bauer, Approximate analytical solutions for the solidification of PCMs in fin geometries using effective thermophysical properties, Int. J. Heat Mass Transf. 54 (23–24) (2011) 4923–4930.
[38] J. Vogel, M. Keller, M. Johnson, Numerical modeling of large-scale finned tube latent thermal energy storage systems, J. Storage Mater. 29 (2020), 101389.
[39] C. Beckermann, R. Viskanta, Natural convection solid/liquid phase change in porous media, Int. J. Heat Mass Transf. 31 (1) (1988) 35–46.
[40] A. Sharma, M. Trivedi, K. Agarwal, N. Nirmalkar, Thermal energy storage in a confined cylindrical heat source filled with phase change materials, Int. J. Heat Mass Transf. 178 (2021), 121603.
[41] R. Pakrouh, M.J. Hosseini, A.A. Ranjbar, A parametric investigation of a PCM-based pin fin heat sink, Mech. Sci. 6 (1) (2015) 65–73.
[42] C. Zhang, et al., Design for laser powder bed additive manufacturing of AlSi12 periodic mesoscale lattice structures, The International Journal of Advanced Manufacturing Technology 113 (11) (2021) 3599–3612.
[43] W. Voigt, Ueber die Beziehung zwischen den beiden Elasticitätsconstanten isotroper Körper, Ann. Phys. 274 (12) (1889) 573–587.
[44] B. Debich, A. El Hami, A. Yaich, W. Gafsi, L. Walha, M. Haddar, Design optimization of PCM-based finned heat sinks for mechatronic components: A numerical investigation and parametric study, J. Storage Mater. 32 (2020), 101960.
[45] S.F. Hosseinizadeh, F.L. Tan, S.M. Moosania, Experimental and numerical studies on performance of PCM-based heat sink with different configurations of internal fins, Appl. Therm. Eng. 31 (17–18) (2011) 3827–3838.
[46] R. Pakrouh, M.J. Hosseini, A.A. Ranjbar, R. Bahrampoury, A numerical method for PCM-based pin fin heat sinks optimization, Energ Convers Manage 103 (2015) 542–552.
[47] P.J. Shamberger, Cooling Capacity Figure of Merit for Phase Change Materials, J. Heat Transfer 138 (2) (2016).
[48] L. Shao, A. Raghavan, G.-H. Kim, L. Emurian, J. Rosen, M.C. Papaefthymiou, T. F. Wenisch, M.M.K. Martin, K.P. Pipe, Figure-of-merit for phase-change materials used in thermal management, Int. J. Heat Mass Transf. 101 (2016) 764–771.
[49] T.J. Lu, Thermal management of high power electronics with phase change cooling, Int. J. Heat Mass Transf. 43 (13) (2000) 2245–2256.
[50] J. Bransier, Stockage periodique par chaleur latente aspects fondamentaux liés a la cinétique des transferts, Int. J. Heat Mass Transf. 22 (6) (1979) 875–883.
[51] M. E. Deckard, J. Felts, and P. J. Shamberger, "Cooling Power and Thermal Buffering in Composite Heatsinks," in *17th IEEE Intersociety Conference on Thermal and Thermomechanical Phenomena in Electronic Systems (ITherm)*, (2018) 109-116.
[52] A. Tamraparni *et al.*, "Design and optimization of composite phase change material for cylindrical thermal energy storage," *In Preparation,* 2022.
[53] R. Waser, F. Ghani, S. Maranda, T.S. O'Donovan, P. Schuetz, M. Zaglio, J. Worlitschek, Fast and experimentally validated model of a latent thermal energy storage device for system level simulations, Appl. Energy 231 (2018) 116–126.
[54] D.R. Askeland, P. Fulay, W. Wright. The science and engineering of materials, 6th edition,", Cengage Learning Inc, 2010.
[55] A. Jayalath, L. Aye, T. Ngo, P. Mendis, Multi-scale analysis on thermal properties of cement-based materials containing micro-encapsulated phase change materials, Constr. Build. Mater. 254 (2020), 119221.
[56] Z. Hashin, S. Shtrikman, A variational approach to the theory of the elastic behaviour of multiphase materials, J. Mech. Phys. Solids 11 (2) (1963) 127–140.
[57] A. Reuss, Berechnung der fließgrenze von mischkristallen auf grund der plastizitätsbedingung für einkristalle, ZAMM-Journal of Applied Mathematics and Mechanics/Zeitschrift für Angewandte Mathematik und Mechanik 9 (1) (1929) 49–58.
[58] H. Zhou, S. Zhang, M. Yang, The effect of heat-transfer passages on the effective thermal conductivity of high filler loading composite materials, Compos. Sci. Technol. 67 (6) (2007) 1035–1040.
[59] D. Li, N. Dai, Y. Tang, G. Dong, Y.F. Zhao, Design and optimization of graded cellular structures with triply periodic level surface-based topological shapes, J. Mech. Des. 141 (7) (2019).
[60] J.M. Hill, One-dimensional Stefan problems: an introduction, Longman Sc & Tech (1987).
[61] V. Alexiades, Mathematical modeling of melting and freezing processes, CRC Press, 1992.
[62] L. M. Jiji , Conduction with Phase Change: Moving Boundary Problems, Heat Conduction, Springer, 2009.
[63] L.M. Jiji, S. Gaye, Analysis of solidification and melting of PCM with energy generation, Appl. Therm. Eng. 26 (5-6) (2006) 568–575.
[64] J. Crepeau, A. Siahpush, Approximate solutions to the Stefan problem with internal heat generation, Heat Mass Transf. 44 (7) (2008) 787–794.
[65] L.S. Yao, W. Cherney, Transient phase-change around a horizontal cylinder, Int. J. Heat Mass Transf. 24 (12) (1981) 1971–1981.